Sini San ameliorates lipid metabolism in hyperprolactinemia rat with liver-depression

Weidong Xu [a,b,*,1], Shasha Tian [a,1], Guanqun Mao [b], Yu Li [a], Hua Qian [b], Wenhua Tao [b]

[a] *School of Pharmacy, Jiangsu University, Zhenjiang, 212013, China*
[b] *Department of Traditional Chinese Medicine, Affiliated Hospital of Jiangsu University, Zhenjiang, 212001, China*

ARTICLE INFO

ABSTRACT

Sini San (SNS) is used to treat liver depression and is applied in both food and herbal medicine. Hyperprolactinemia (HPRL) is a common endocrine disorder, and patients with HPRL are usually associated with depressive symptoms. However, whether SNS is effective in treating HPRL combined with liver depression and its underlying mechanisms are unknown. We applied network pharmacology and molecular docking to predict the mechanism of SNS for the treatment of liver-depressed HPRL. Therapeutic effects were validated in animal models and cells. Metabolomics was also used to evaluate the effect of SNS on liver-depressed HPRL. Network pharmacology and molecular docking analysis showed that AKT1, TNF and IL6 were the key targets, and SNS improved depressive behaviors, regulated sex hormone levels, and improved ovarian morphology. Combined network pharmacology and metabolomics analyses showed that SNS could act by regulating lipid metabolism. In addition, SNS significantly reduced the release of prolactin (PRL) in rat pituitary tumor MMQ cells. Overall, SNS can significantly treat HPRL liver depression at both animal and cellular levels, and effectively alleviate the related symptoms by regulating lipid metabolism. AKT1, TNF and IL6 may be key targets.

1. Introduction

Hyperprolactinemia (HPRL) is a common endocrine disease in women and is characterized by serum prolactin (PRL) levels that are persistently higher than the upper limit of normal. PRL serves as the main biomarker for the diagnosis of HPRL (Mastnak et al., 2023). HPRL is a significant contributor to the condition of infertility, may cause patients to experience weight gain, delayed pubertal development, galactorrhea, hypogonadism and reduced fertility (Bernard et al., 2015), alongside various other medical disorders and factors, collectively impacting approximately 8–12 percent of individuals within the childbearing age group globally (Vander Borght and Wyns, 2018). The specific hormonal effects involve increased PRL levels, decreased levels of FSH and LH, and reduced levels of estrogen and progesterone, all of which primarily disrupt the balance of the hypothalamic-pituitary-ovarian axis (H. Zhang et al., 2016).

Studies have shown some interconnectivity between polycystic ovary syndrome and HPRL, with mild HPRL in patients with polycystic ovary syndrome, with a prevalence of 11%–17% (Kim et al., 2023). Thus, HPRL also has a major impact on the physiological function of the ovary, inhibiting aromatase activity in follicular granulosa cells, leading to a decrease in estrogen synthesis and thus inhibiting follicular development and maturation (Hummel et al., 1990). Clinical studies have also found that HPRL patients have higher depression, anxiety and stress scores than controls (De Sousa et al., 2020). HPRL patients are often accompanied by mental health challenges, such as depression, hostility, irritability, and anxiety. In reality, 75–90% of diseases are closely linked to chronic psychosocial stress, encompassing conditions like depression and mood disorders (W. Wang et al., 2023).

Carbamazepine and bromocriptine are used as first-line drugs for the treatment of symptomatic HPRL, but systematic reviews and meta-analyses have shown that their efficacy is unsatisfactory, with the main problems being post-treatment relapse rates (30%–80%), drug resistance and patient intolerance (Zeng et al., 2023). Therefore, exploring and developing novel therapeutic strategies is crucial to improve the clinical management of patients with HPRL.

Sini San (SNS), a medicinal food formula, first recorded by Zhang Zhongjing in "Treatise on Miscellaneous Diseases of the Typhoid Fever", has the efficacy of dispersing the liver and relieving depression, harmonizing the spleen and stomach, and is often used in the treatment of depression and other liver-qi stagnation syndromes (Zhu et al., 2023).

Abbreviations

AKT1	Serine/Threonine kinase AKT1
BRO	bromocriptine mesylate
CASP3	Caspase 3
GO	gene ontology
HE	hematoxylin-eosin
HPRL	hyperprolactinemia
IL1B	Interleukin 1β
IL6	Interleukin 6
JUN	Jun proto-oncogene
KEGG	Kyoto Encyclopedia of Genes and Genomes
LC-MS/MS	liquid chromatography-tandem mass spectrometry
MMP9	Matrix metalloproteinase 9
OFT	open field test
OPLS-DA	orthogonal partial least squares discriminant analysis
PCA	principal components analysis
PPI	Protein-Protein Interaction Networks
PRL	prolactin
PTGS2	Prostaglandin-endoperoxide synthase 2
QC	quality control
SNS	Sini San
SPT	sugar water preference test
STAT3	Signal transducer and activator of transcription 3
TNF	Tumor necrosis factor
TP53	Tumor protein P53
TST	tail suspension test
UPLC-Q-Exactive Orbitrap/MS	ultra-high performance liquid chromatography coupled with hybrid quadrupole-orbitrap mass spectrometry
VIP	Variable Importance in Projection

This prescription consists of four medicinal herbs: *Radix Bupleuri, Radix Paeoniae Alba, Fructus Aurantii Immaturus,* and *Glycyrrhizae Radix et Rhizoma*, three of which can be used in both food and medicine (L. Ye et al., 2023). Modern research shows that SNS can effectively treat depression and other mental diseases through its multi-component, multi-target, and multi-system pharmacological effects (H. Wang et al., 2022). At this time, no studies have definitively confirmed the efficacy of SNS in the treatment of HPRL, either at the clinical or basic research level. Given the need for improved first-line treatment options for HPRL, it is particularly significant to investigate the therapeutic potential of SNS for HPRL, especially since there is a wealth of experience in using SNS to treat endocrinological gynecological diseases associated with HPRL (L. Liu et al., 2019; Zheng et al., 2021).

Network pharmacology studies have revealed the core active ingredients of SNS in treating depression, including flavonoids such as isorhamnetin, formononetin, and naringenin, and steroidal compounds such as stigmasterol, Beta-sitosterol and sitosterol. KEGG pathway enrichment analyses suggest that SNS may play a role in the treatment of depression through neuroactive ligand-receptor interactions, 5-hydroxytryptaminergic synaptic pathways, dopaminergic synaptic pathways, and GABAergic synaptic pathways (H. Wang et al., 2022). Animal experiments have confirmed that SNS can alleviate depressive-like behaviors caused by CUMS (M. J. Zhang et al., 2023). In addition, SNS can also improve depressive-like behavior in rats by regulating mitochondrial function and synaptic plasticity(Deng et al., 2022). Although there are certain similarities in treatment strategies between HPRL and depression, and SNS has shown good efficacy in treating depression, it is unclear whether SNS can treat HPRL. Conventional therapy has shown limitations in the treatment of HPRL,The therapeutic effects of SNS in alleviating liver qi stagnation could potentially introduce novel approaches to the treatment of HPRL, especially in the field of female infertility. In view of this, it is particularly important to deeply investigate the effects of SNS on liver-depressive HPRL and its mechanism of action.

Metabolomics, as a "top-down" analytical approach, is uniquely suited to reveal the overall changes in metabolic levels of complex metabolic diseases. This method provides a comprehensive perspective for understanding the overall function of living systems by comprehensively analyzing downstream metabolites and their interaction pathways in the body. This is consistent with the holistic view advocated by traditional Chinese medicine, which emphasizes the interconnection and coordination and balance between various parts of the body (Xiao et al., 2023). Metabolomics has been widely used in the field of diagnosis and treatment of depression. A large amount of research literature shows that by analyzing the metabolome of patients, specific metabolic markers related to depression can be discovered, thereby providing new

perspectives and strategies for the diagnosis and treatment of the disease (X. Liu et al., 2023). In addition, metabolomics has also been used to evaluate the therapeutic effect of traditional Chinese medicine compounds on liver diseases such as fatty liver, liver fibrosis, and liver failure. These studies not only reveal the pharmacological mechanism of traditional Chinese medicine compounds, but also provide scientific basis for clinical treatment (S. Zhang et al., 2023). However, there is currently a lack of metabolomic research on the treatment of HPRL with liver-depression. Therefore, using metabolomics methods to study the metabolic characteristics of HPRL with liver-depression is expected to reveal the underlying mechanism of the disease and provide a direction for finding new treatment strategies.

This study uses CUMS combined with metoclopramide-induced HPRL rat model of liver-depression and rat MMQ cells that secrete large amounts of PRL. It aims to use serum metabolomics, network pharmacology, molecular docking simulations and cell experiments to explore the therapeutic effect and mechanism of SNS on HPRL with liver-depression type.

2. Materials and methods

2.1. Chemicals and reagents

Methanol (chromatography grade, Merck, German), formic acid (chromatography grade, Aladdin, China), acetonitrile (chromatography grade, Merck, German); metoclopramide injection (Tianjin Jinyao Pharmaceutical Co., Ltd.), bromocriptine mesylate tablets (Gedeon Richahter Plc.), bromocriptine mesylate (Shanghai Aladdin Biochemical Technology Co.,Ltd., 99%), Rat E_2 ELISA kit, Rat FSH ELISA kit (Hunan Aifang Biotechnology Co., Ltd.); rat MMQ cell (Procell Life Science&Technology Co.,Ltd.), Specialized medium for MMQ cells (Procell Life Science&Technology Co.,Ltd.),Cell Counting Kit-8 (New Cell & Molecular Biotech Co.,Ltd.), Rat PRL ELISA kit (animal experiment: Hunan Aifang Biotechnology Co., Ltd., cell experiment: Shanghai Enzyme Linked Biotechnology Co., Ltd.).

2.2. Preparation of SNS water decoction

Radix Bupleuri (batch number: 230220, source: Zhangjiagang Green Chinese Herbs Medicine Co., Ltd.), *Fructus Aurantii Immaturus* (batch number: A230414, Source: Bozhou Baishixin Traditional Chinese Medicine Pieces Co., Ltd.), *Glycyrrhizae Radix et Rhizoma* (batch number: 220601, source: Bozhou Baishixin Traditional Chinese Medicine Pieces Co., Ltd.), *Radix Paeoniae Alba* (batch number: 230501, source: Bozhou Baishixin Traditional Chinese Medicine Pieces Co., Ltd.). The identification of all the herbs was done by Prof. Ouyang Zhen from Jiangsu

University to ensure the quality and purity of the herbs.

According to the General Principles of Chinese Medicinal Preparations of the Pharmacopoeia of the People's Republic of China, SNS is prepared as follows: first, weigh 6 g of each of *Radix Bupleuri, Radix Paeoniae Alba, Fructus Aurantii Immaturus*, and *Glycyrrhizae Radix et Rhizoma*, and add 10 times the volume of water to soak for 1 h. Then, bring the mixture to a boil, then maintain it at 100° for 40 min, stirring occasionally to ensure even heating. After the decoction was completed, the mixture was allowed to cool naturally and the filtrate was filtered through 8 layers of gauze to separate the dregs and collect the filtrate. Next, the dregs were decocted for a second time by adding 8 times the volume of water, bringing to a boil, and then maintaining it at 100°for 40 min. After the decoction was completed, it was cooled again and filtered through 8 layers of gauze to retain the liquid. The filtrates obtained from the two decoctions were combined and concentrated to contain 0.8 g/mL raw herb. Finally, the concentrated liquid was stored in a refrigerator at 4 °C for subsequent use (Shen et al., 2020; Xu et al., 2022).

2.3. Preparation of SNS-medicated serum

Twenty SPF-grade male SD rats, 200–220 g, were purchased from Jiangsu University Animal Center, were acclimatized for one week. Twenty rats were evenly distributed into a control group and an experimental group, of 10 rats each. Referring to the "Pharmacology Experimental Methodology", with the equivalent dose conversion of 60 kg adult, the administered dose of SNS for rats was 2 g/kg, and the administered concentration of SNS was 0.2 g/mL at the dose of 1 mL per 100 g gavage for rats, once a day. In order to obtain a greater blood concentration, twice the clinical dosage was selected as the final dosage concentration of SNS (0.4 g/mL) (Xu et al., 2022).

After SD rats were acclimatized, the control group was given physiological saline, and the SNS group was given SNS decoction for 7 days. The subjects were fasted and water-free 12 h before preparing to collect blood. The blank group and experimental group were anesthetized 2 h after the last dose and blood was collected from the abdominal aorta. Rats were anesthetized using 1% sodium pentobarbital (40 mg/kg). The collected blood was allowed to stand for half an hour and the supernatant was centrifuged at 1500 rpm for 8–10 min. The serum was allowed to stand in a water bath at 56 °C for half an hour, filtered through a 0.22 μm filter to remove bacteria, and stored in a refrigerator at −80 °C.

2.4. Component analysis of SNS water decoction, SNS-medicated serum

Dilute 200 μL of water decoction with 800 μL of methanol, vortex for 1 min, extract with ultrasonic for 20 min, and centrifuge at 13000 rpm for 15 min. The supernatant was filtered through a 0.22 μm microporous membrane. The pre-treatment method of SNS-medicated serum and the blank serum are the same as that of the decoction of SNS.

Ultra-high performance liquid chromatography coupled with hybrid quadrupole-orbitrap mass spectrometry (UPLC-Q-Exactive Orbitrap/MS) system from Thermo Fisher Scientific, USA, equipped with a HYPERSIL GOLD C18 column (2.1 mm × 100 mm, 1.9 μm), was used to analyze the various constituents in water decoction of SNS, drug-containing serum of SNS, and blank serum.

Chromatographic conditions: The mobile phase A was the water solution of 0.1% formic acid, while the mobile phase B was the acetonitrile solution. The column temperature in positive ion mode was 45 °C, and the column temperature in negative ion mode was 30 °C. Flow rates were both 0.35 mL/min, and the injection volume was 5 μL. Gradient elution program: 0–0.5 min, 2% B; 0.5–3.0 min, 2%–30% B; 3.0–5.0 min, 30%–70% B; 5.0–14.0 min, 70%–98% B; 14.0–16.0 min, 98% B; 16.0–16.1 min, 98%–2% B; 16.1–19.0 min, 2% B.

Mass spectrometry conditions: Ion source: ESI; mass spectrometry scanning range: 100.0–1000.0 m/z; sheath gas flow rate was 49 Arb, auxiliary gas flow rate was 12 Arb, auxiliary gas heating temperature

was 350 °C; spray voltage was 3.2kv; capillary temperature was 320 °C; S-lens RF voltage was 50 V.

2.5. Pharmacodynamic study of SNS on rats with HPRL with liver-depression

2.5.1. Animals

60 female Sprague–Dawley rats (225–250 g body weight), aged 6–8 weeks, were provided by Zhejiang Vital River Laboratory Animal Technology Co., Ltd. (Certificate No.: 20230222Aazz0619000362). After the animals arrived, they were placed in the Laboratory Animal Research Center of Jiangsu University (SYXK(SU)2023-0081) and acclimated to the environment under appropriate feeding conditions for 1 week. All animal experiments in this studies were approved by the Institutional Animal Care and Use Committee of Jiangsu University (Approval number: UJS-IACUC-2023022401).

Rats were housed in a 12-h light/dark cycle environment with 50%–60% humidity and 22–25 °C temperature. Rats had free access to food and water throughout the experimental period, except during modeling and during sucrose intake testing. Rats were kept under specific pathogen-free conditions to ensure the accuracy and reliability of the experiments.

Before the experiment, the rats were randomly divided into six groups, namely: CON group (Group A), positive control group (Group B), LOW-SNS group (Group C), MID-SNS group (Group D), HIGH-SNS group (Group E) and MODEL group (Group F), 10 in each group. The CON group refers to the control group, which consists of rats that have not received any administered drugs. The MODEL group refers to the model group, composed of rats that were induced by CUMS and subcutaneous injections of metoclopramide hydrochloride.

2.5.2. Experimental design

In order to construct a HPRL model with liver-depression, this study adopted a staged approach. During the first three weeks of the experiment, rats were subjected to CUMS to construct a state of liver-depression. In addition, metoclopramide was injected on Day 1 - Day 10 to induce HPRL. In the 4th week, in order to evaluate the effectiveness of the model, PRL was measured and a series of behavioral tests were conducted, including sugar water preference test (SPT), tail suspension test (TST), and open field test (OFT). From the 5th to the 8th week, the successfully modeled rats were treated with bromocriptine mesylate(BRO) and different doses of SNS. In the 9th week, behavioral tests of rats were conducted again, including SPT, TST, and OFT. The overall timeline of the pharmacodynamic experiment in rats is shown in Fig. S1a.

HPRL with low-depressison model was induced by CUMS combined with subcutaneous injection of metoclopramide as follows. From day 1 of modeling, rats in group B, C, D, E, and F received subcutaneous injections of metoclopramide at a dose of 50 mg/kg of body weight once daily for 10 days (Q. Ye et al., 2010; H. Zhang et al., 2016). At the same time, rats in groups B, C, D, E, and F received the following stimuli from the first day of modeling: stimulating odor (1 min each time), restraint (2 h each time), food deprivation (24 h each time), water deprivation (24 h each time), wet bedding (24 h each time), tail clamping (1 min each time), once a day for a total of 21 days. Rats in group A did not receive any stimulation, but for control purposes, an equal amount of saline was injected subcutaneously at a dose of 50 mg/kg of body weight daily for 21 days.

Specific stimulation methods were as follows: stimulating odor: spraying 30% glacial acetic acid solution for 1 min; food deprivation: removing feed for 24 h; water deprivation: removing water bottle for 24 h; wet bedding: soaking and moistening the bedding in the cage with water for 24 h; tail clamping: using a tail clip tool to hold the rat's tail 2 cm from the tip of the tail for 1 min (Y. Yang et al., 2024).

Rats with unsuccessful modeling were excluded. Rats in each group were given corresponding drugs or distilled water through gastric

feeding once a day for 28 days. The rats in group A and F were gastrically fed with an equal volume of 0.9% aqueous sodium chloride solution; the rats in group B were gastrically fed with 1 mg/kg/d of BRO solution, and 0.9% aqueous sodium chloride solution was used as a solvent (Q. Ye et al., 2010; H. Zhang et al., 2016); Group C (LOW-SNS group) was 2 g/kg SNS; Group D (MID-SNS group) was 4 g/kg SNS; Group E (HIGH-SNS group) was 8 g/kg SNS. The rats were fed once a day for 4 weeks for 28 days. The experimental protocol was approved and adopted by the Animal Use and Management Committee of Jiangsu University.

2.5.3. Behavioral test

2.5.3.1. Sugar water preference test.
After rats adapted to 1% sucrose solution and ordinary water for 12 h, SPT was performed. To prevent animals from preferring drinking locations, the order of water bottles was changed once in the middle. After the training period, remove food and water. After 12 h of food and water deprivation, two water bottles were placed in separate rat cages, one containing 1% sucrose solution and the other containing ordinary water. The rats drank freely within 1 h, the consumption of sucrose solution and ordinary water was measured, and the sucrose preference rate was calculated. The calculation formula of sucrose preference rate is: sucrose preference percentage = (sucrose consumption/(sucrose consumption + ordinary water consumption)) × 100% (Zhao et al., 2024).

2.5.3.2. Tail suspension test.
The rat's tail (2 cm from the tip of the tail) was suspended from a hook on the horizontal bar of the tail suspension test device with adhesive tape for 7 min, with the first 2 min being the acclimatisation time. The cumulative duration of the rat's immobility during the 5-min period was recorded. The rat was considered immobile when it stopped struggling and remained completely still.

2.5.3.3. Open field test.
Before the start of the test, every rat was placed in the OFT box to adapt for 2 min. During the experiment, the rat was placed in the center of the test box and allowed to move freely for 5 min. The activity of the rats was recorded over a 5 min period, including movement time and total distance traveled. After each trial, the test chamber was thoroughly cleaned using 75% ethanol to remove any residual olfactory cues. The environment was kept quiet during the experiment (M. Zhang et al., 2022).

The above behavioral tests were all completed at the Experimental Animal Center of Jiangsu University. Through these behavioral tests, the cognitive function and emotional state of rats under the HPRL model with liver-depression can be evaluated, as well as the effect of SNS on these functions.

2.5.4. Sample collection

The rats were treated with food deprivation, but with water, 12 h prior to blood collection. Two hours after the last administration, rats were anesthetized with 1% sodium pentobarbital (40 mg/kg), and blood was collected through the abdominal aorta into pre-numbered tubes. The blood samples were allowed to stand at room temperature and then centrifuged at 1500 rpm for 10 min to obtain the supernatant. The rats were dissected under ice bath conditions to obtain the ovaries as well as the hypothalamus. These tissues were rapidly transferred to liquid nitrogen for freezing and stored in a refrigerator at −80 °C until further use. The ovaries were fixed in paraformaldehyde for HE-stained section preparation.

2.5.5. Biochemical testing

In order to evaluate the effectiveness of the rat model, in addition to behavioral experiments on rats, this study also detected PRL content in the peripheral serum of rats after drug modeling. After drug treatment, the PRL, E_2, and FSH content in the serum were also measured. All samples were analyzed directly according to Elisa kit instructions, and the detection of each sample was repeated three times to ensure the accuracy and reliability.

2.5.6. Hematoxylin-eosin staining

The right ovaries of rats were fixed using 4% paraformaldehyde, embedded in paraffin, and subsequently sectioned at a thickness of 5 μm. These sections were then stained with HE (hematoxylin-eosin) for routine histological examination, following which a comprehensive morphological assessment and analysis of the ovarian tissue was conducted via light microscopy.

2.6. Metabolomic analysis of serum of rats with liver-depression HPRL

Blood was collected from CON group (Group A), positive control group (Group B), LOW-SNS group (Group C), MID-SNS group (Group D), HIGH-SNS group (Group E) and MODEL group (Group F) and the serum was collected after centrifugation and stored at −80 °C for non-targeted metabolome assay.

After the sample is melted on ice, 300 μL of extraction solution containing internal standard (acetonitrile: methanol = 1:4, volume ratio) is added and vortexed for 10 s. Add 50 μL sample and 300 μL extraction solution into a 2 mL tube, vortex for 3 min, and centrifuge at 12,000 rpm for 10 min at 4 °C. Collect 200 μL of the supernatant and place it at −20 °C for 30 min, followed by centrifugation at 12,000 rpm for 3 min at 4 °C. Transfer 180 μL of supernatant to liquid chromatography-tandem mass spectrometry (LC-MS/MS).

LC-MS/MS analysis was performed on a Shimadzu LC-30A ultra-high performance liquid chromatograph with Triple TOF 6600 quadrupole tandem time-of-flight mass spectrometer. samples were analyzed using a T3 column (Waters ACQUITY Premier HSS T3 Column 1.8 μm, 2.1 mm * 100 mm), using 0.1% formic acid aqueous solution as solvent A and 0.1% formic acid acetonitrile as solvent B. Elute according to the following gradient: 0–2.0 min, 5%–20% B; 2.0–5.0 min, 20%–60% B; 5.0–6.0 min, 60%–99% B; 6.0–7.5 min, 99% B; 7.5–7.6 min, 99 % to 5% B; 7.6–10.0 min, 5% B. The analysis conditions are as follows: ion source, ESI; column temperature, 40 °C; flow rate, 0.4 mL/min; injection volume, 4 μL. Samples had the same elution gradient in negative ion conditions as in positive ion mode.

The source parameters are set as follows: ion source gas 1, 50 psi; ion source gas 2, 50 psi; curtain gas, 25 psi; temperature, 550 C; normal deflection potential, 60 V, −60 V in positive and negative; ion spray, 5000 V or −4000V. The TOF MS scanning parameters: mass range, 50–1000Da; the product ion scanning parameters: mass range, 25–1000Da.

Principal component analysis (PCA) and orthogonal partial least squares discriminant analysis (OPLS-DA) were used to perform dimensionality reduction analysis to demonstrate the differences in metabolite composition between samples. Metabo Analyst 5.0 was used to perform functional pathway enrichment and topology analysis to screen differential metabolic molecules. The identified metabolites were annotated using the KEGG compound database and then mapped to the KEGG pathway database. Significantly enriched pathways in a given metabolite list were identified using p-values from the hypergeometric test.

2.7. Network pharmacology of SNS in treating HPRL with liver depression

The TCMSP platform was used to search for 4 herbal ingredients with oral availability ≥30% and drug-likeness ≥0.18, and the active ingredients were searched for the targets of single drug components by their MOL. ID numbers (Ru et al., 2014). Use the Uniprot database to download the Excel data sheet of the compounds, optimize the data using the "TRIM" function, and use the "VLOOKUP" function to match the target gene names. Finally, the target proteins of the chemical compositions obtained by the above methods were annotated using the Uniprot database (Dimmer et al., 2012). Invalid components with no

target at the screening point.

Disease target information related to "depression, hyperprolactinemia" was obtained from GeneCards and OMIM databases (Stelzer et al., 2016). All the targets were integrated, the duplicate genes were eliminated, and the disease targets were merged. Finally, the Venny software was used to obtain the intersection of the targets of the components of SNS and the targets of HPRL and liver-depression, which are the potential targets of SNS for the treatment of HPRL with liver-depression.

Using Cytoscape 3.9.0 software, import relevant files, perform network topology analysis, and adjust the target graphics, color, transparency and size according to degree value, so as to construct the network diagram of "herbal ingredients-targets-diseases" (Shannon et al., 2003).

The potential target in the treatment of liver-depressed HPRL were obtained by importing intersecting genes into the String platform, setting the target as homo sapiens, taking the highest confidence level of 0.900, and hiding the free gene nodes (Szklarczyk et al., 2019). The results were imported into Cytoscape 3.9.0 software to make Protein-Protein Interaction Networks (PPI) maps, and the top 10 core targets were filtered according to the degree value.

Bioconductor was used to install within the R software to analyze Gene Ontology (GO) and Kyoto Encyclopedia of Genes and Genomes (KEGG) functional enrichment of biological processes and visualize them through the microbiology platform (L. Chen et al., 2015; Ogata et al., 1999). The top 10 GO terms and the top 20 KEGG pathways were visualized and analyzed according to the P value.

The protein structure of the core target was retrieved from PDB database (https://www.rcsb.org/). The core protein was then dehydrated and cleaved. Chemical structures of the drugs were obtained from the TCMSP database in PDB format. Docking simulations were conducted using Autodock, and the results were subsequently visualized in PyMOL.

2.8. Cell experiments

MMQ pituitary tumor cells were cultured in a complete culture medium containing 10% horse serum, 5% fetal calf serum plus streptomycin and penicillin. Keep temperature of the incubator at 37 °C, the CO_2 concentration at 5%, and the air humidity at 95 %. The cells grow in suspension (Tang et al., 2019).

Cells in the logarithmic phase are taken for experiments. After cell counting, they were inoculated into 96-well cell culture plates were cultured for 24, 48, and 72 h respectively. Add 10 μL of CCK8 reagent to each well and incubate at 37 °C for 1 h, 2 h, and 3 h. Measure the absorbance at 450 nm using a microplate reader.

Take the logarithmic phase MMQ cell, adjust the number of cells to 5×10^5 cells/mL, pipet evenly, and inoculate it into 96-well plates. The experimental group and blank group wells were diluted cell suspension, and the solvent group wells was cell-free culture medium, 90 μL/well, with 3 multiple wells, and placed in an incubator for 24 h. Different concentrations of BRO (3.75, 7.5, 15, 30, 60, 75 μg/mL) and different concentrations of drug-containing serum (5%, 10%, 15%, 20%, 25%) were added to the experimental group wells. An equal volume of complete culture medium was added to the blank group wells. After 24 h, 48 h, and 72 h of treatment, 10 μL of CCK-8 reagent was added to each well, incubated at 37 °C for 2 h, and the absorbance was measured at a wavelength of 450 nm with a microplate reader, and cell viability was calculated. Cell viability = (OD value of experimental group - OD value of solvent group)/(OD value of blank group - OD value of solvent group) × 100%. In order to eliminate the influence of self-contained substances in serum and DMSO on cell viability, 10%, 20% normal serum, and DMSO groups were used as control in the drug-containing serum concentration selection experiment.

The logarithmic phase MMQ cell was inoculated into a 6-well plate at 5×10^5 cells/mL, 1.5 mL/well, with 3 multiple wells, and starved for 24

h. Different concentrations of BRO (3.75, 7.5, 15 μg/mL) were added to the experimental group wells, and an equal amount of cell-free culture medium was added to the blank group wells. After 24 h of treatment, MMQ cell suspension was collected, and the supernatant was collected after centrifugation. Store at −80 °C and avoid repeated freezing and thawing. Follow the instructions of the ELISA kit to detect PRL levels.

The logarithmic phase MMQ cell was inoculated into a 6-well plate at 5×10^5 cells/mL, 1.5 mL/well, with 3 multiple wells, and starved for 24 h. Different concentrations of drug-containing serum (5%, 10%, 20%) and the optimal concentration of BRO were added to the experimental group wells, and an equal amount of cell-free culture medium was added to the blank group. After 24 h of treatment, the MMQ cell suspension was collected, and the supernatant was collected after centrifugation. Store at −80 °C and avoid repeated freezing and thawing. Follow the instructions of the ELISA kit to detect PRL levels.

2.9. Data processing and analysis

Statistical analysis was conducted using GraphPad Prism 9.0.1. Independent t-tests were used for comparisons between two groups, while one-way ANOVA and Tukey's multiple comparisons were applied for comparisons among three or more groups. $P < 0.05$ was considered significant. Data are presented as mean ± SEM.

3. Results

3.1. Identification of chemical components of SNS water decoction

SNS water decoction, SNS-medicated serum, and blank serum were examined using UPLC-Q-TOF-MS technique, aiming at qualitatively analysing the composition of SNS chemical components in vivo and ex vivo, so as to clarify the material basis of this compound formula. The total ion chromatograms of SNS decoction, SNS drug serum and blank serum in positive and negative ion mode are shown in Fig. S1. This analytical approach led to the identification of 42 chemical constituents within SNS water decoction, encompassing flavonoids, terpenes, phenylpropanoids, organic acids, and coumarins. These constituents were elucidated under both positive and negative ion modes, with 16 constituents detected in the positive ion mode and 26 in the negative ion mode, predominantly consisting of original compounds (Table 1). These chemical constituents predominantly originate from various Chinese herbal medicines, with specific attribution as follows: 5 constituents from *Radix Bupleuri*, 8 from *Radix Paeoniae Alba*, 12 from *Aurantii Fructus Immaturus*, and 9 from *licorice*, 1 shared between *Radix Bupleuri* and *Radix Paeoniae Alba*, 1 common to *adix Bupleuri*, *Radix Paeoniae Alba*, and *licorice*, 3 shared between *Radix Bupleuri* and *licorice*, and 2 common to *Aurantii Fructus Immaturus* and *licorice*.

In the blank serum control, three primary components of SNS water decoction—linoleic acid, formononetin, and myristic acid—were detected in SNS-medicated serum. Some metabolites were also noted, but they have not yet been subjected to detailed investigation.

3.2. Pharmacodynamic studies

3.2.1. HPRL model with liver-depression was successfully constructed

After a 21-day treatment of CUMS in combination with metoclopramide, PRL levels of rats in the model group 1–5 were significantly elevated compared with the CON group (Fig. S2b).

In order to assess the modelling effect, behavioural experiments including SPT, TST and OFT were conducted for assessing pleasure lack, anxiety-depressive state and autonomous exploration ability, respectively. Compared with the CON group, rats in MODEL group 1–5 exhibited a significantly reduced sucrose preference rate in the SPT (Fig. S2c), and The immobility time in TST significantly increased (Fig. S2d). Additionally, both the movement time and total movement distance in the OFT were markedly decreased (Figs. S2e–2f). These

Table 1
Identification of chemical constituents in SNS water decoction by UPLC-Q-Exactive Orbitrap/MS.

Serial number	Chemical Name	Formula	m/z	RT [min]	Reference Ion	Source
1	Fraxetin	$C_{10}H_8O_5$	208.03691	5.431	Neg	Radix Bupleuri
2	Hyperoside	$C_{21}H_{20}O_{12}$	464.09563	5.27	Neg	Radix Bupleuri
3	Kaempferitrin	$C_{27}H_{30}O_{14}$	578.16423	5.968	Neg	Radix Bupleuri
4	Linoleic acid	$C_{18}H_{32}O_2$	280.2404	12.739	Neg	Radix Bupleuri
5	Puerarin	$C_{21}H_{20}O_9$	416.11504	7.136	Pos	Radix Bupleuri
6	Benzoylpaeoniflorin	$C_{30}H_{32}O_{12}$	601.21678	6.313	Pos	Paeonia Radix Alba
7	1_2_3_4_6-Pentakis-O-galloyl-beta-D-glucose	$C_{41}H_{32}O_{26}$	940.11879	5.353	Neg	Paeoniae Radix Alba
8	albiflorin	$C_{23}H_{28}O_{11}$	480.16341	4.351	Pos	Paeoniae Radix Alba
9	Catechin	$C_{15}H_{14}O_6$	290.07932	4.28	Neg	Paeoniae Radix Alba
10	Catechol	$C_6H_6O_2$	110.03574	3.595	Neg	Paeoniae Radix Alba
11	Methyl gallate	$C_8H_8O_5$	184.03651	3.583	Neg	Paeoniae Radix Alba
12	Paeoniflorin	$C_{30}H_{32}O_{12}$	480.16377	5.672	Neg	Paeoniae Radix Alba
13	Salicylic acid	$C_7H_6O_3$	138.03077	4.458	Neg	Paeoniae Radix Alba
14	Apigenin	$C_{15}H_{10}O_5$	270.05314	6.715	Neg	Aurantii Fructus Immaturus
15	Bergapten	$C_{12}H_8O_4$	216.0425	6.578	Pos	Aurantii Fructus Immaturus
16	Eriocitrin	$C_{27}H_{32}O_{15}$	596.17433	5.844	Neg	Aurantii Fructus Immaturus
17	Hesperetin	$C_{16}H_{14}O_6$	302.07901	6.526	Neg	Aurantii Fructus Immaturus
18	Hesperidin	$C_{28}H_{34}O_{15}$	610.18913	4.844	Pos	Aurantii Fructus Immaturus
19	Limonin	$C_{32}H_{42}O_{14}$	650.25825	5.283	Neg	Aurantii Fructus Immaturus
20	Luteolin	$C_{15}H_{10}O_6$	286.04798	6.652	Neg	Aurantii Fructus Immaturus
21	Nobiletin	$C_{21}H_{22}O_8$	402.13169	8.127	Pos	Aurantii Fructus Immaturus
22	Obacunone	$C_{26}H_{30}O_7$	454.19937	7.379	Pos	Aurantii Fructus Immaturus
23	Poncirin	$C_{28}H_{34}O_{14}$	594.1954	5.96	Pos	Aurantii Fructus Immaturus
24	Rhoifolin	$C_{27}H_{30}O_{14}$	578.16417	5.274	Pos	Aurantii Fructus Immaturus
25	Tangeritin	$C_{20}H_{20}O_7$	372.12099	8.911	Pos	Aurantii Fructus Immaturus
26	18-β-Glycyrrhetinic acid	$C_{30}H_{46}O_4$	470.33969	9.423	Pos	Licorice
27	Formononetin	$C_{16}H_{12}O_4$	268.07374	6.885	Neg	licorice
28	Glabridin	$C_{20}H_{20}O_4$	324.13648	9.501	Pos	licorice
29	Glabrone	$C_{20}H_{16}O_5$	336.10002	8.198	Neg	licorice
30	Glycyrrhizin	$C_{42}H_{62}O_{16}$	822.40415	8.416	Neg	licorice
31	Isoliquiritigenin	$C_{15}H_{12}O_4$	256.07366	5.572	Pos	licorice
32	Medicarpin	$C_{16}H_{14}O_4$	270.08946	6.733	Neg	licorice
33	Methylnissolin-3-O-glucoside	$C_{23}H_{26}O_{10}$	462.15016	5.373	Pos	licorice
34	Ononin	$C_{22}H_{22}O_9$	476.13234	6.163	Neg	licorice
35	Vicenin II	$C_{27}H_{30}O_{15}$	594.1591	4.372	Pos	licorice
36	Myristic acid	$C_{14}H_{28}O_2$	228.20868	11.946	Neg	Radix Bupleuri、Paeoniae Radix Alba
37	Kaempferol	$C_{15}H_{10}O_6$	286.04781	5.715	Pos	Radix Bupleuri、Paeoniae Radix Alba、licorice
38	Isorhamnetin	$C_{16}H_{12}O_7$	316.05858	6.698	Neg	Radix Bupleuri、licorice
39	Quercetin	$C_{15}H_{10}O_7$	302.04271	6.353	Neg	Radix Bupleuri、licorice
40	Rutin	$C_{27}H_{30}O_{16}$	610.1562	6.128	Neg	Radix Bupleuri、licorice
41	Naringenin	$C_{15}H_{12}O_5$	272.06877	6.464	Neg	Aurantii Fructus Immaturus、licorice
42	Naringin	$C_{27}H_{32}O_{14}$	580.17941	5.814	Neg	Aurantii Fructus Immaturus、licorice

behavioral changes collectively indicate the increase depressive-like behaviors in the MODEL group, suggesting the successful establishment of a model of liver-depression HPRL.

3.2.2. SNS improves depressive-like behavior in HPRL rats with liver-depression

The sucrose preference rate of rats in the SPT was upregulated after SNS treatment compared to the MODEL group (Fig. 1a). Compared with the MODEL group, the immobility time of rats in the TST was significantly shorter after SNS treatment (Fig. 1b). Rats treated with SNS showed a significant increase in moving time and total moving distance in the OFT (Figs. 1c-2d). The results show that the depressive-like behaviors of the SNS group were improved in different degrees compared with the MODEL group.

### 3.2.3. SNS improves the level of sex hormones in HPRL

Following induction, significant alterations in sex hormone concentrations (PRL, E_2, and FSH) were observed in liver-depressed HPRL rats. Notably, serum PRL levels were markedly elevated (Fig. 1e) and FSH levels exhibited a downward trend (Fig. 1f). Additionally, E_2 levels were significantly reduced (Fig. 1g) in the model group compared to the CON group. Treatment with SNS subsequently led to significant improvements in the levels of PRL, E_2, and FSH, suggesting that SNS exerts a positive regulatory effect on the sex hormone profiles of liver-depressed HPRL rats.

3.2.4. SNS improves ovarian tissue morphology in HPRL rats with liver-depression

HPRL significantly impacts the physiological functions of the ovaries, consequently leading to pronounced morphological changes in the ovaries following the induction of the model. In the CON group, a large number of follicular cells of different developmental stages were seen in the ovarian tissue, with normal follicular structure, thick granulosa cell layer and tight arrangement (Fig. 2a). In the model group, follicular atresia was observed in the ovarian tissue of the rats, the number of cystic follicles was increased, the granulosa cell layer was thinned out and loosely arranged, and luteolysis was reduced or disappeared (Fig. 2b). The degree of ovarian lesions was relieved in all dose groups and BRO group, and the ovarian morphology was close to that in the MID-SNS group and BRO group (Fig. 2c–f). In the above mentioned cases, the degree of ovarian lesions was alleviated in the MID-SNS group and BRO group, with a similar ovarian morphology.

3.3. Rat serum metabolomic analysis

Serum metabolites from each group of rats were systematically analyzed using LC-MS/MS in conjunction with multivariate statistical methods to pinpoint metabolites exhibiting significant changes pre- and post-treatment. The results of both total ion chromatography (Fig. 3a) and unsupervised PCA (Fig. 3b) showed that the quality control (QC) samples exhibited stability throughout the experiments, reflecting the high stability of the instrument and the excellent reproducibility of the
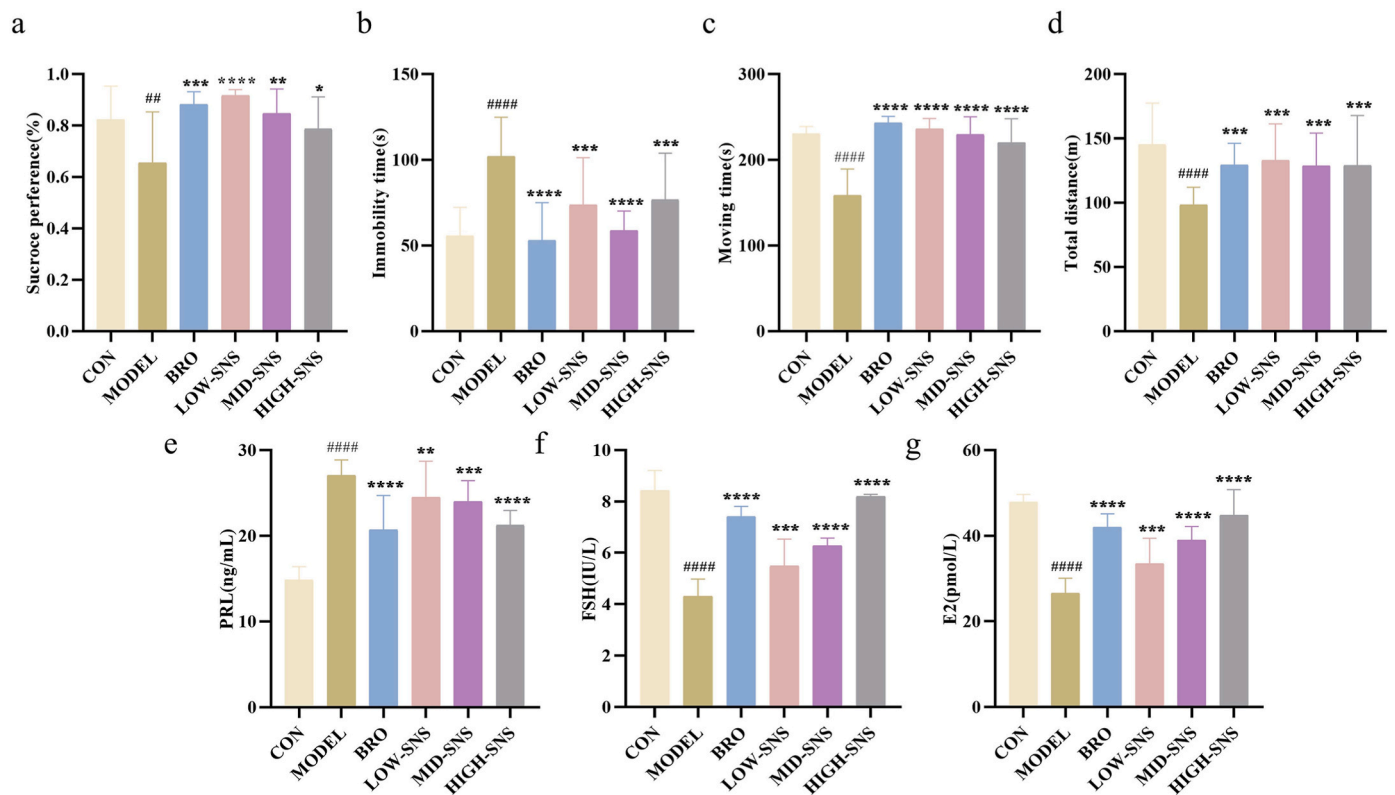
Fig. 1. SNS improves the depression-like behavior of liver-depressed HPRL rats. (a) Sugar water preference test. (b) Tail suspension test. (c-d) Open field test. (e) PRL levels in rats. (f) FSH levels in rats. (g) E_2 content in rats. Data are mean ± standard deviation, n = 6. Compared with the CON group, *$p < 0.05$, **$p < 0.01$, ***$p < 0.001$, ****$p < 0.0001$. Compared with the MODEL group, ##$p < 0.01$, ####$p < 0.0001$.
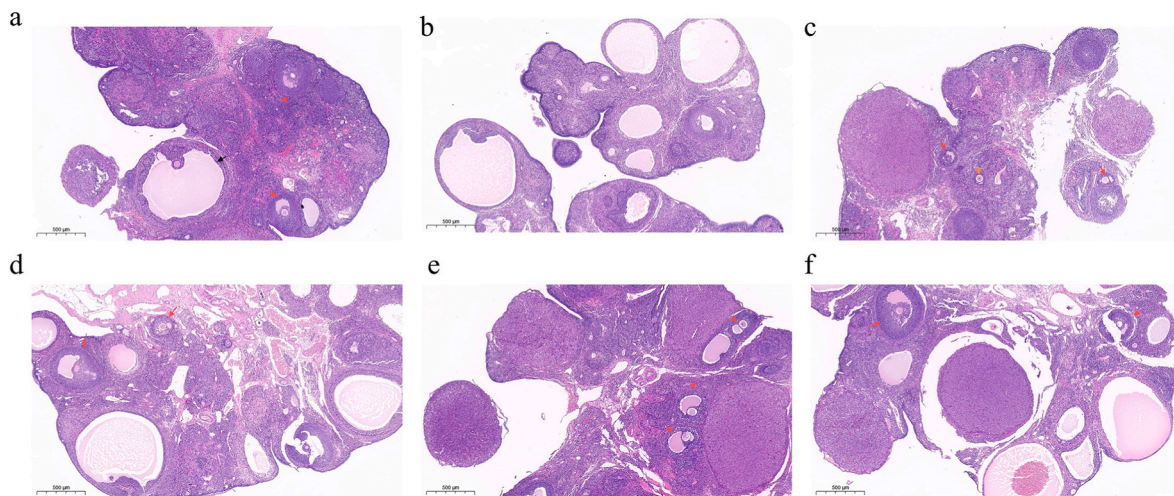

Fig. 2. SNS improved ovarian histomorphology in HPRL rats with liver-depression. (a) Normal group. (b) Model group. (c) BRO group. (d) LOW-SNS group. (e) MID-SNS group. (f) HIGH-SNS group. Scale bar = 500 μm. Yellow arrow represents primary follicles, red arrow represents secondary follicles, and black arrow represents mature follicles.

LC-MS/MS technique. A total of 3302 metabolites were identified by LC-MS/MS technique, including 1156 in negative ion mode and 2146 in positive ion mode.

In the unsupervised PCA analysis, the separation trend between the six groups of samples in positive and negative ion modes was clearly demonstrated. Notably, the LOW-SNS and MID-SNS groups were located between the CON and MODEL groups in both ion modes, whereas the HIGH-SNS group was between the CON and MODEL groups in the positive mode, and closer to the MODEL group and deviated from the

CON group in the negative mode (Lim et al., 2021). These results strongly suggest that SNS treatment can effectively regulate the abnormal metabolic pattern of liver-depression HPRL rats. For further validation, OPLS-DA was then employed, and this analysis showed that the CON and the MODEL group showed a significant separation from each other (Fig. 3c) (M. Liu et al., 2024), suggesting that the serum metabolic profiles of the rats were significantly altered as a result of the model induction. In addition, there was a statistically significant separation between the SNS groups and the MODEL group (Fig. 3d–g).
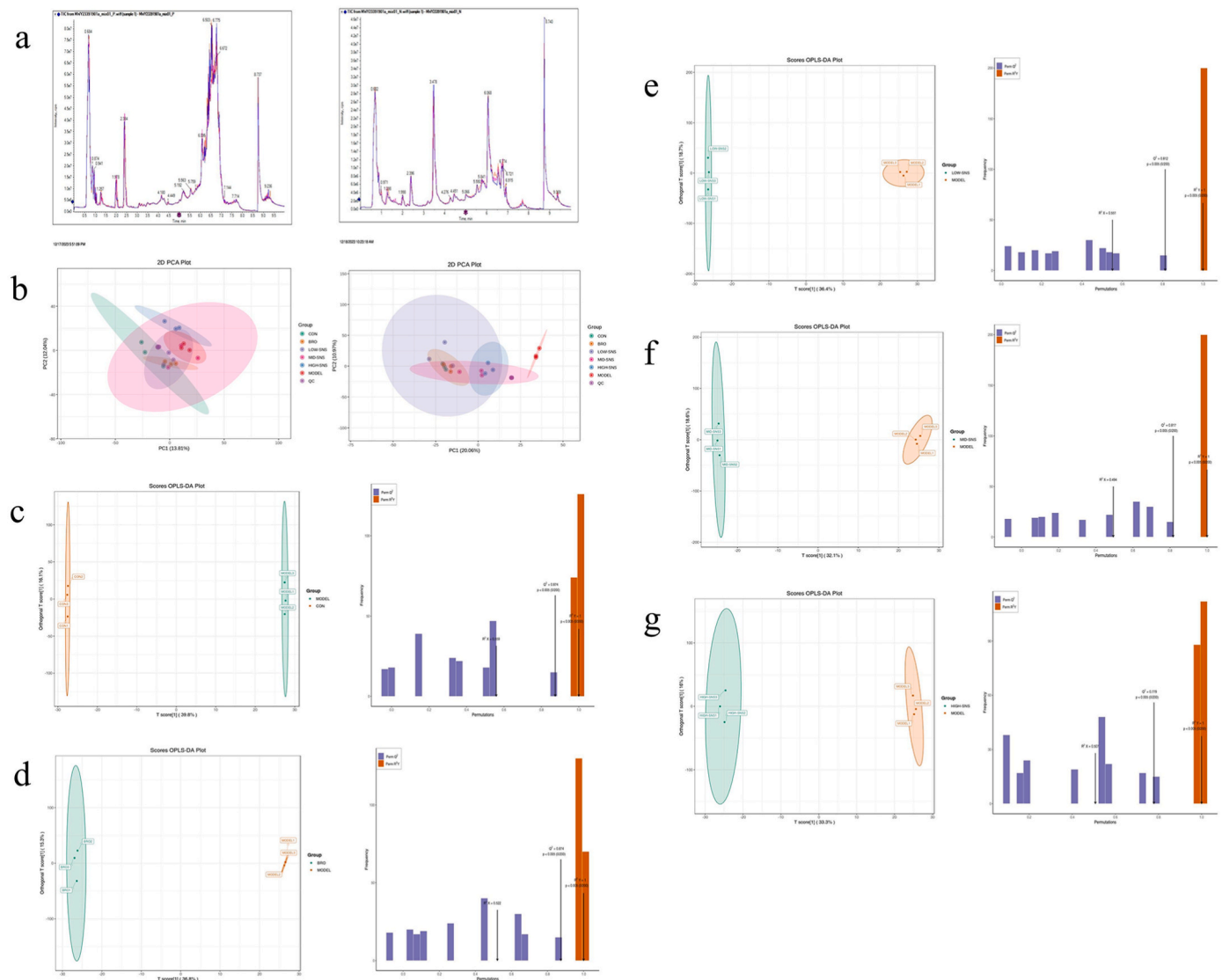
Fig. 3. Statistical analysis of serum samples. OPLS-DA score plots for the former, and OPLS-DA validation plots for the latter. (a) Total ion flow plots in positive and negative ion modes. (b) PCA plots of samples in each group in positive and negative ion modes. (c) MODEL group vs. CON group (d) BRO group vs. MODEL group.(e) LOW-SNS group vs. MODEL group. (f) MID-SNS group vs. MODEL group. (g) HIGH-SNS group vs. MODEL group.

Differential metabolites were initially pinpointed using the criteria of a Variable Importance in Projection (VIP) value ≥ 1 and a p-value <0.05 (Su et al., 2019), signifying substances that exhibit a reversed expression trend following SNS treatment when compared to the modeling phase. Relative to the MODEL group, the LOW-SNS group experienced up-regulation of 255 metabolites and down-regulation of 117, amounting to 372 differential metabolites. The MID-SNS group witnessed up-regulation of 192 and down-regulation of 118, totaling 310 differential metabolites. In the HIGH-SNS group, 240 metabolites were up-regulated and 80 were down-regulated, summing up to 320 differential metabolites (Fig. 4a–c). Venn Online software was employed for a collective analysis of the differential metabolites across the three groups, disclosing 157 metabolites commonly altered among all groups (Fig. 4d). Subsequent refinement of these 157 metabolites based on more stringent criteria—VIP value ≥ 1, p-value <0.01, and a fold change (FC) of ≥3 or ≤ 0.33—led to the identification of 44 potential biomarkers, including 43 up-regulated and a single down-regulated differential metabolite (Fig. 4e). Comprehensive details of the identified differential metabolites in serum are provided in Table 2.

A heatmap was employed to visualize the alterations in the 44 differential metabolites (Fig. 5a), while violin plots were utilized to depict the trends in their concentration levels (Fig. 5b). To avoid confusion due to the length of certain compound names, abbreviations MW0151979, MW0016978, and MW0103099 have been utilized. MW0151979 is Methanone, (1-pentyl-1H-indol-3-yl)(4-propyl-1-naphthalenyl)- and MW0016978 is [(2S,3R,4S,5S,6R)-6-[[(2R,3R,4R,5S,6R)-3,4-dihydroxy-6-(hydroxymethyl)-5-[(2S,3R,4R,5R,6S)-3,4,5-trihydroxy-6-methyloxan-2-yl]oxyoxan-2-yl]oxymethyl]-3,4,5- trihydroxyoxan-2-yl] (1S, 2R,4aS,6aR,6aS,6bR,8R,8aR,10R,11R,12aR,14bS)-8,10,11-trihydroxy-1,2,6a,6b,9,9,12a-heptamethyl-2,3,4,5,5,6a,7,8,8a,10,11,12,13,14b-tetradecahydro-1H-picene-4a-carboxylate. MW0103099 is (2S,3R,4S,5S,6R)-2-[(2R,3R,4S,5S,6R)-2-[(3S,5R,8R,9R. 10R,12R,13R,14R,17S)-17-[(2S)-5,6-dihydroxy-6-methyl-2-[(2S,3R,4S,5S,6R)-3,4,5-trihydroxy-6-(hydroxymethyl)oxan-2-yl]oxyheptan-2- yl]-12-hydroxy-4,4,8,10,14-pentamethyl-2,3,5,6,7,9,11,12,13,15,16,17-dodecahydro-1H-cyclopenta[a]phenanthren-3-yl]oxy]-4,5- dihydroxy-6-(hydroxymethyl)oxan-3-yl]oxy-6-(hydroxymethyl)oxane-3,4,5-triol. The restoration of metabolic profiles for these differential metabolites indicates that SNS treatment effectively mitigates metabolic disorders, primarily through the upregulation of metabolite levels.

To elucidate the metabolic pathways influenced by SNS, enrichment analysis of the altered metabolites was conducted using the KEGG
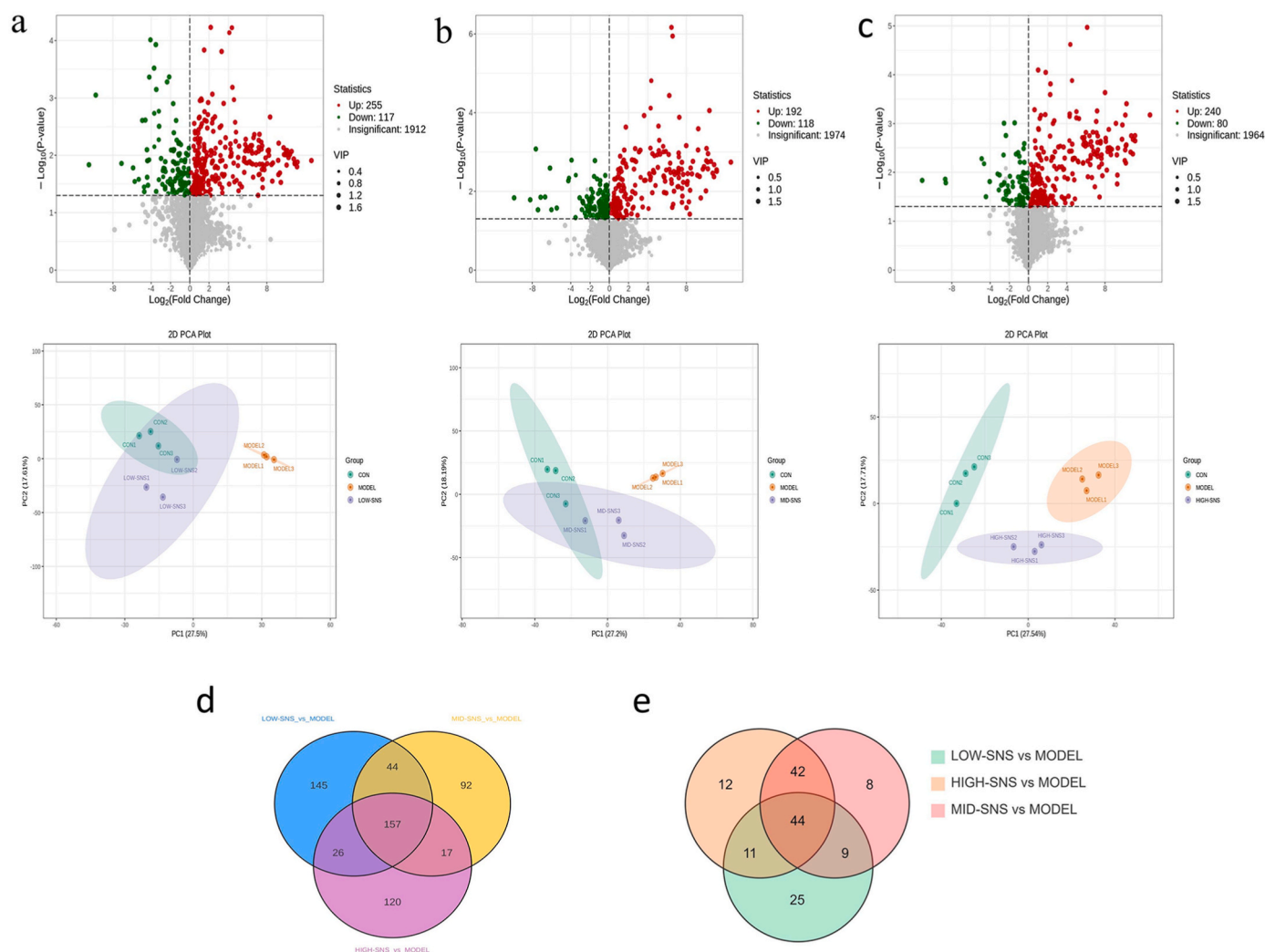
Fig. 4. Screening of differential metabolites. (a) LOW-SNS group vs. MODEL group. (b) MID-SNS group vs. MODEL group. (c) HIGH-SNS group vs. MODEL group. The first row shows the volcano plot and the second row shows the PCA score plot. (d) Venn diagram of differential metabolites between the three groups a-c under conditions of VIP value ≥ 1 and p-value < 0.05. (e) Venn diagram of differential metabolites between the three groups a-c under the conditions of VIP value ≥ 1, p-value < 0.01, FC ≥ 3 or FC ≤ 0.33.

database. This analysis identified 17 enriched metabolic pathways (Fig. 5c), predominantly involving glycerophospholipid metabolism, glycerolipid metabolism, fat digestion and absorption, and vitamin digestion and absorption.

3.4. Network pharmacology analysis of SNS in treating HPRL with liver-depression

Through the TCMSP database, SNS was found to contain 138 active ingredients, specifically including 17 from *Radix Bupleuri*, 7 from *Paeoniae Radix Alba*, 22 from *Aurantii Fructus Immaturus*, and 92 from *Licorice*. The effective targets for these constituents included 136 for *Radix Bupleuri*, 69 for *Paeoniae Radix Alba*, 209 for *Aurantii Fructus Immaturus*, and 1500 for *Licorice*. After deduplication, the total number of unique effective targets for SNS was determined to be 240.

The top 5 Degree ranked active ingredients of SNS are quercetin, kaempferol, beta-sitosterol, naringenin, and luteolin (Fig. 6a). The targets for depression and HPRL were screened by searching the OMIM and Gene Cards databases, totaling 14,841 targets after removing duplicates. Intersecting these targets with targets for SNS, 231 common targets were finally identified (Fig. 6b). The intersections of SNS components and disease-related targets were entered into the STRING database for network analysis. The results showed that the PPI network included 63

nodes and 1664 edges (Fig. 6c). Analysis revealed the top 10 key targets, which included Serine/Threonine kinase AKT1 (AKT1), Tumor Necrosis Factor (TNF), Interleukin 6 (IL6), Tumor protein P53 (TP53), Interleukin 1β (IL1B), Prostaglandin-Endoperoxide Synthase 2 (PTGS2), Signal Transducer and Activator of Transcription 3 (STAT3), Jun proto-oncogene (JUN), Caspase 3 (CASP3), and Matrix metalloproteinase 9 (MMP9) (Fig. 6d). The component-target-disease network diagram is shown (Fig. 6e).

KEGG enrichment analysis yielded 189 catalogs with a p-value of <0.05. The top 20 pathways with the highest significance were represented in a bubble diagram for visualization (Fig. 6f). The results showed that the main target focuses of SNS for the treatment of liver-depression HPRL, such as Lipid and atherosclerosis, AGE-RAGE signaling pathway in diabetic complications, Hepatitis B. A total of 4556 entries for biological progress, 360 entries for cellular components, and 619 entries for molecular functions were obtained in the GO analysis enrichment. The top 10 of screened biological progress, cellular components, and molecular functions were made into a bar graph for presentation (Fig. 6g). Combining the results of network pharmacology and untargeted metabolomics for the metabolic pathway of KEGG, it can be concluded that the metabolic pathway for the treatment of liver-depressive HPRL by SNS may be lipid metabolism.

Five active components were docked with five potential targets. The

Table 2
Differential metabolites identified in rat serum untargeted metabolomics techniques.

Compounds	Formula	RT (min)	Adduct	LOW-SNS_vs_MODEL_Type	MID-SNS_vs_MODEL_Type	HIGH-SNS_vs_MODEL_Type
Ranolazine	$C_{24}H_{33}N_3O_4$	4.0415	$[M + NH_4]^+$	up	up	up
Carvedilol	$C_{24}H_{26}N_2O_4$	2.9046	$[M + H-H_2O]^+$	up	up	up
Phytolaccoside E	$C_{42}H_{66}O_{16}$	4.2518	$[M + H-H_2O]^+$	up	up	up
Veratrine	$C_{32}H_{49}NO_9$	3.7955	$[M + NH_4]^+$	up	up	up
Thalicarpine	$C_{41}H_{48}N_2O_8$	3.7253	$[M+H]^+$	up	up	up
Ginsenoside RG2	$C_{42}H_{72}O_{13}$	3.9538	$[M+]^+$	up	up	up
Prenoxdiazine	$C_{23}H_{27}N_3O$	3.8834	$[M + NH_4]^+$	up	up	up
Saikosaponin A	$C_{42}H_{68}O_{13}$	3.8483	$[M+]^+$	up	up	up
Alpha-Solanin	$C_{45}H_{73}NO_{15}$	3.965	$[M+H]^+$	up	up	up
Metergoline	$C_{25}H_{29}N_3O_2$	3.91184	$[M+H]^+$	up	up	up
1-O-Hexadecyl-lyso-sn-glycero-3-phosphocholine	$C_{24}H_{52}NO_6P$	6.8282	$[M+H]^+$	up	up	up
Westiellamide	$C_{27}H_{42}N_6O_6$	3.6026	$[M + NH_4]^+$	up	up	up
Gymnemic acid I	$C_{43}H_{66}O_{14}$	3.9538	$[M + H-H_2O]^+$	up	up	up
MG(18:1/0:0/0:0)	$C_{21}H_{40}O_4$	5.9858	$[M+H]^+$	down	down	down
His-Arg-Lys-Glu	$C_{23}H_{40}N_{10}O_7$	3.6026	$[M+H]^+$	up	up	up
Glu-Arg-Glu	$C_{16}H_{28}N_6O_8$	3.1112	$[M+H]^+$	up	up	up
His-Asn-Phe-Lys	$C_{25}H_{36}N_8O_6$	3.8658	$[M+H]^+$	up	up	up
Gly-Leu-Arg-Val-Phe	$C_{28}H_{46}N_8O_6$	3.6902	$[M+H]^+$	up	up	up
Arg-Ser-Trp	$C_{20}H_{29}N_7O_5$	3.9538	$[M+H]^+$	up	up	up
Tyr-Phe-Lys-Ile-Asp	$C_{34}H_{48}N_6O_9$	4.094	$[M+H]^+$	up	up	up
MW0151979	$C_{27}H_{29}NO$	3.9538	$[M+H]^+$	up	up	up
Met-Lys-Lys	$C_{17}H_{35}N_5O_4S$	3.9911	$[M + NH_4]^+$	up	up	up
Trp-Ala-Lys	$C_{20}H_{29}N_5O_4$	3.9009	$[M + NH_4]^+$	up	up	up
His-Arg-Tyr-Arg	$C_{27}H_{42}N_{12}O_6$	3.6375	$[M+H]^+$	up	up	up
Phe-Leu-Phe	$C_{24}H_{31}N_3O_4$	3.9559	$[M + NH_4]^+$	up	up	up
His-Lys-Ser	$C_{15}H_{26}N_6O_5$	3.7955	$[M+H]^+$	up	up	up
Asn-Arg-Ala	$C_{13}H_{25}N_7O_5$	3.7955	$[M+H]^+$	up	up	up
Gln-Ile-Val-Glu	$C_{21}H_{37}N_5O_8$	4.059	$[M + H-H_2O]^+$	up	up	up
LPA(i-24:0/0:0)	$C_{27}H_{55}O_7P$	7.0238	$[M + NH_4]^+$	up	up	up
Psychotrin	$C_{28}H_{36}N_2O_4$	4.0065	$[M+H]^+$	up	up	up
Tragopogonsaponin L	$C_{50}H_{74}O_{15}$	4.3395	$[M + H-H_2O]^+$	up	up	up
Phe-Tyr-Lys-Arg	$C_{30}H_{44}N_8O_6$	3.6902	$[M+H]^+$	up	up	up
Arg-Asp-Leu-Tyr-Ser	$C_{28}H_{44}N_8O_{10}$	3.6552	$[M+H]^+$	up	up	up
Ile-Leu-Tyr-Asp	$C_{25}H_{38}N_4O_8$	3.8131	$[M+H]^+$	up	up	up
Lys-Cys-Val-Ala-Phe	$C_{26}H_{42}N_6O_6S$	3.9009	$[M+H]^+$	up	up	up
Val-Ile-Leu-Asp	$C_{21}H_{38}N_4O_7$	3.4275	$[M + NH_4]^+$	up	up	up
Phe-Lys-Glu-Ala-Phe	$C_{32}H_{44}N_6O_8$	4.024	$[M+H]^+$	up	up	up
Arg-Glu-Lys-Asp-Lys	$C_{27}H_{50}N_{10}O_{10}$	3.7253	$[M + NH_4]^+$	up	up	up
Ser-His-Val-Lys	$C_{20}H_{35}N_7O_6$	4.0765	$[M + NH_4]^+$	up	up	up
Phe-Leu-Val-Gly-Gly	$C_{24}H_{37}N_5O_6$	4.1115	$[M+H]^+$	up	up	up
MW0016978	$C_{48}H_{78}O_{19}$	4.3746	$[M + H-H_2O]^+$	up	up	up
Leu-Arg-Asp-Lys	$C_{22}H_{42}N_8O_7$	4.2342	$[M+H]^+$	up	up	up
Ritterazine A	$C_{54}H_{76}N_2O_{10}$	4.0065	$[M+]^+$	up	up	up
MW0103099	$C_{48}H_{84}O_{20}$	4.3923	$[M + H-H_2O]^+$	up	up	up

binding energy, which is more negative for stronger interactions, indicates the predicted affinity of the ligand for the target in molecular docking. The five active components of SNS (quercetin, kaempferol, beta-sitosterol, naringenin, and luteolin) exhibited varying degrees of binding to AKT1, TNF, IL6, TP53, IL1B, PTGS2, STAT3, JUN, CASP3, and MMP9, which were represented in heatmap (Fig. 7a). The results indicated that quercetin, kaempferol, beta-sitosterol, naringenin, and luteolin exhibit high affinity for AKT1, TNF, and IL6, with a slightly weaker affinity of −4.3 between naringenin and IL6. TP53 and kaempferol had the highest affinity of −7.6 and IL1B and affinity beta-sitosterol had the highest of −7.4. Overall, quercetin had a high affinity for AKT1, TNF, IL6. The most stable combinations were chosen and visualized, representing small molecules and proteins with enhanced binding capabilities (Fig. 7b-f).

3.5. SNS reduces the content of PRL released by MMQ cells

Cell absorbance decreased under different time incubation conditions as cell density reached a certain threshold (Fig. 8a-c). The optimal inoculum densities and incubation time for achieving higher absorbance were determined to be were 5, 2.5, and 1×10^5/mL and 24 h, 48 h, and 72 h. Given the cost of time, subsequent experiments utilized an inoculum density of 5×10^5/mL and a 24-h incubation period. The addition of CCK8 reagent was followed by a 2-h incubation.

After incubating MMQ cells with SNS-containing serum at various concentrations for 24, 48, and 72 h, cell viability was assessed using the CCK8 assay. The results indicated a marked increase in cell survival rates in the 5%, 10%, and 15% drug-containing serum groups relative to the blank control and normal serum groups. In contrast, treatment with 10% and 20% blank serum for 24 h led to significant inhibition of cell viability (Fig. 8d). To ensure that there was no inherent inhibitory effect of the containing serum on MMQ cell viability, and taking into account

Fig. 5. Comparison of differences in the content of differential metabolites and their metabolic pathway analysis. (a) Clustering heat map of differential metabolites. (b) Differential metabolite relative content violin plot. 3 of the 44 differential metabolites have too long names and are replaced with codes. (c) KEGG enrichment analysis of differential metabolites. The color of the dot is the P-value size, the redder indicates the more significant enrichment.The size of the dot represents the number of different metabolites enriched.

the cost of the drug and time, concentrations of 5%, 10% and 20% of the containing serum and a 24-h treatment were chosen for further experimental studies.

Following the incubation of MMQ cells with BRO at various concentrations for 24, 48, and 72 h, cell viability was measured using the CCK8 assay. The results indicated that 1‰ DMSO had no impact on cell viability after 48 and 72 h of treatment. To confirm that BRO itself does not inhibit MMQ cell viability and considering the cost and time required, concentrations of 3.75, 7.5, and 15 μg/mL BRO were selected for 24-h treatment in subsequent experiments (Fig. 8e). The PRL content was significantly reduced after treatment with different concentrations of BRO, with 7.5 μg/mL BRO being chosen for the subsequent control positive drug study (Fig. 8f). Compared to the blank group, the PRL content in the BRO group and the SNS-containing serum at each dose was significantly reduced (Fig. 8g), suggesting that SNS reduces PRL content in a dose-dependent manner, thus indicating its potential in treating HPRL.

4. Discussion

The qualitative analysis has successfully elucidated the 42 active constituents of the SNS formulation, the majority are prototypical. Experimental validation has confirmed that SNS administration significantly ameliorates depressive behaviors, normalizes sex hormone levels, and restore of ovarian tissue morphology in affected rats. Through Network pharmacology and molecular docking assessment, key targets such as AKT1, TNF, and IL6 have been identified for the management of

liver-depression HPRL. Metabolomic profiling has uncovered 44 differential metabolites. By comprehensive analysis, SNS treatment was performed through lipid metabolism. Moreover, SNS potently suppresses the secretion of prolactin from rat pituitary tumor cells.

We successfully constructed the "HPRL rat model with liver depression", which is a multifactorial composite model that combines the characteristics and symptoms of the disease under the guidance of Chinese medicine theory (Z. Li et al., 2022). In the theory system of Chinese medicine, the cause of liver depression is mainly related to the depression of liver qi caused by emotional depression and emotional stimulation.

Currently, there are various methods for preparing animal models of liver depression evidence (Bai et al., 2021), among which CUMS, as a non-invasive stimulus, successfully constructed liver depression evidence by subjecting rats to long-term CUMS, which puts them in a long-term state of anxiety and tension, and became one of the classic methods for preparing this model (J. Liu et al., 2022). SPT, OFT, and TST are commonly used to assess depressive behaviors in rodents (Y. Liu et al., 2023; Xu et al., 2022). The SPT measures the animal's emotional state by evaluating its preference for sweet tastes. The OFT observes the animal's exploration and social interactions in an open environment. The TST evaluates the sense of depression by recording the animal's struggling activities while the tail is suspended. In this study, the animal model of liver-related depression exhibited decreased preference for sugar water, reduced locomotor activity, and extended periods of immobility during the TST. The pharmacodynamic assessment revealed that various doses of SNS significantly ameliorated the depressive-like

Fig. 6. Network pharmacological analysis of SNS in the treatment of liver-depression HPRL. (a) Core active ingredients of SNS. (b) Venn diagram depicting the Intersection of SNS active compounds and disease targets. (c) Protein interaction network diagram. (d) Core target genes. (e) Traditional Chinese medicine ingredient-target-disease network diagram. (f) GO analysis of the core target genes, Molecular Function, Biological Process, and Cellular Component. (g) Enrichment analysis of the KEGG pathway of the core target genes.

behaviors in the model group.

Several methods have been reported to establish HPRL animal models, with subcutaneous metoclopramide injection being the most commonly used, along with intraperitoneal injection (Araujo et al., 2023; Wei et al., 2017). Currently, most researchers believe that dopamine is the most dominant and potent prolactin-inhibiting factor secreted by the hypothalamus, directly inhibiting PRL release (Gragnoli et al., 2016). As a dopamine D_2 receptor antagonist, metoclopramide blocks DA from binding to its receptor, thus preventing DA's inhibitory effect on PRL, leading to PRL overproduction (Baranoglu Kilinc, Torun and Kilinc, 2024). A commonly used drug regimen to induce HPRL is to administer 50 mg/kg metoclopramide hydrochloride daily for 10 days (H. Zhang et al., 2016). This method is cost-effective and widely adopted in research. Additionally, some researchers have developed an HPRL animal model by implanting pituitary tissue from hyperprolactinemic rats into the kidney capsule of female rats (Moreno-Carranza et al., 2013). Another study successfully induced HPRL in rats by continuous risperidone administration, resulting in elevated serum PRL levels, this is becausea common side effect of antipsychotic medications during administration is the potential induction of HPRL (Zhai et al., 2024).

In this study, a marked elevation in serum PRL levels were achieved by subcutaneously administering 50 mg/kg of metoclopramide to rats

over a period of 10 consecutive days, thus effectively replicating the primary clinical characteristics of HPRL. Furthermore, the research utilized the CUMS to induce a depressive state in the rats. The integration of the HPRL model with the depression model is a less documented approach in the scientific literature, highlighting the novelty of the study design.

The current study also uncovered disturbances in FSH and E_2 levels and abnormal histopathological changes in ovarian tissue in rats subjected to the modeling treatment. Increasing evidence indicates a strong association between liver-depression HPRL and sex hormone dysregulation (Szukiewicz, 2024; H. Zhang et al., 2016). On one hand, liver-depression HPRL may lead to sex hormone disorders. On the other hand, these disorders may exacerbate the symptoms of liver-depression HPRL. Specific effects of HPRL on the reproductive endocrine system include suppression of ovarian function (Szukiewicz, 2024). That elevated serum PRL levels interfere with follicular development and maturation, resulting in decreased ovulation frequency and reduced egg quality. Furthermore, HPRL disrupts the normal functioning of the hypothalamic-pituitary-gonadal axis, influencing the synthesis and release of gonadotropin-releasing hormone and consequently reducing sex hormone secretion. This inhibitory effect on sex hormones can disrupt follicle maturation and development, affecting the fertilization
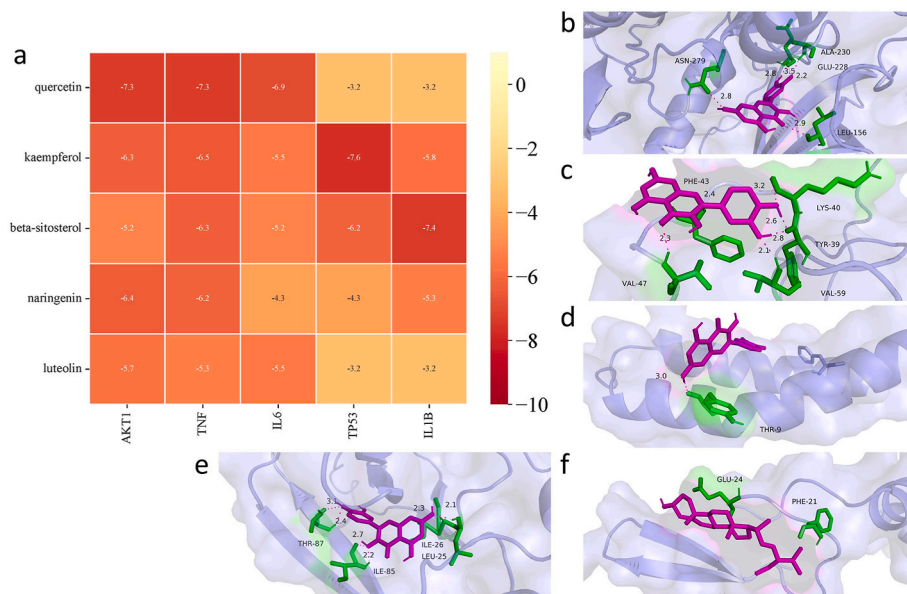
Fig. 7. Molecular docking simulation. (a) Heat map of molecular docking. (b) The binding of AKT1 with quercetin. (c) The binding of TNF with quercetin. (d) The binding of IL6 with quercetin. (e) The binding of TP53 with kaempferol. (g) The binding of IL1B with beta-sitosterol.
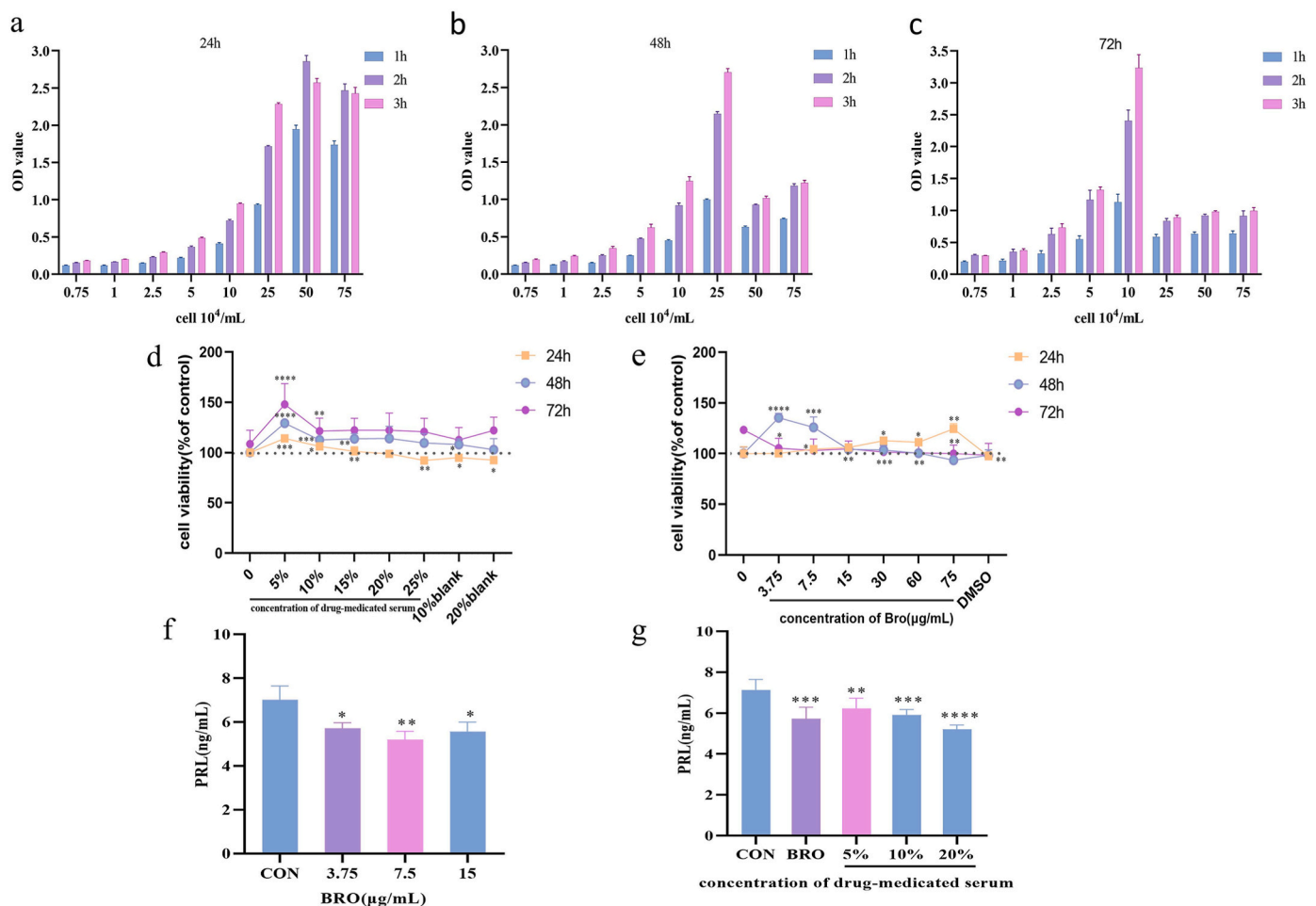
Fig. 8. Serum from rats containing SNS significantly reduces the content of PRL released by MMQ cells. (a-c) Effects of different incubation times, inoculation densities, and CCK8 incubation times on the activity of MMQ cells. (d) Effects of different concentrations of drug-containing serum on the viability of MMQ cells. (e) Effects of different concentrations of bromocriptine mesylate on the viability of MMQ cells. (f) Effects of BRO on the content of PRL released by MMQ cells. (g) Effects of SNS-containing serum on the content of PRL released by MMQ cells in rats. Data are mean ± standard deviation, n = 4. *$p < 0.05$, **$p < 0.01$, ***$p < 0.001$, ****$p < 0.0001$ compared with the CON group (drug concentration = 0).

process and embryo development, potentially leading to menstrual irregularities, amenorrhea, or infertility. Therefore, when treating HPRL, the comprehensive consideration of its effects on the reproductive endocrine system, particularly ovarian function and sex hormone balance, is essential. Through comprehensive therapeutic strategies, the restoration of endocrine balance, the alleviation of symptoms, and the enhancement of quality of life can be achieved. For example, Pterostilbene, one homologous derivative of resveratrol, can exert therapeutic effects on HPRL by mediating the balance of apoptosis and anti-apoptosis in ovarian and uterine tissues, inhibiting serum PRL levels, and regulating the secretion of reproductive hormones (H. Zhang et al., 2016). Bu-Shen-Zhu-Yun decoction enhances the CSN5-GATA1 interaction, promoting PRLR deubiquitination and activating the JAK2/STAT5 pathway, thereby upregulating kisspeptin, a peptide hormone encoded by the KISS-1 gene, to treat hyperprolactinemia-related infertility by modulating female reproductive endocrine functions (Feng et al., 2021).

In addition, this study used UPLC-Q-Exactive Orbitrap/MS technology to analyze the composition of the decoction of SNS, qualitatively identifying more prototypical components of the traditional Chinese medicine and ensuring the source of the pharmacodynamic substances. A variety of compounds possess anti-inflammatory properties. PRL exhibited dual regulation of IL-1β and TNF-α in mouse synovial fibroblasts: upregulation of long PRL receptors by IL-1β and downregulation by TNF-α. PRL attenuated the proinflammatory effects of IL-1β and NF-κB activation but enhanced TNF-α-triggered inflammatory responses and NF-κB signaling (García-Rodrigo et al., 2023). It is speculated that the anti-inflammatory components of SNS are able to modulate the relationship between PRL and inflammatory factors by some mechanism. Furthermore, certain substances have been identified as exhibiting potent antidepressant effects, including hyperoside, linoleic acid, and albiflorin. These compounds have been found to directly target and alleviate symptoms of liver depression induced by CUMS.

MMQ cells exhibit a robust capacity for PRL secretion, making them a valuable tool for investigating the biosynthesis and secretion mechanisms of PRL, as well as its role in the physiological and pathological states of mammals. This experiment's findings indicate that SNS-containing serum could significantly diminish the prolactin content in the supernatant of MMQ cells, with the effect being comparable to that of BRO. MMQ cells are a suitable cellular model for HPRL.

The first 3 key targets, namely AKT1, TNF, and IL6, were obtained by Network Pharmacology and molecular docking. Programmed necrosis is an unnatural mode of cell death regulated by intracellular signals(Zorzi and Bonvini, 2011). TNF-α is thought to be one of the key factors that initiate programmed necrosis (Q. Zhang et al., 2023). It has been shown that elevated TNF-α in the hypothalamus of HPRL model rats may cause programmed necrosis and damage dopaminergic neurons. And TNF is also inextricably linked to depression (L. Chen et al., 2024). It has been shown that TNF levels are usually significantly elevated in the peripheral blood of depressed patients (Tian et al., 2023). TNF-α may be involved in the pathophysiological process of depression through a variety of mechanisms, including activation of the hypothalamic-pituitary-adrenal axis (Ben-Azu et al., 2023), stimulation of the neuronal 5-hydroxytryptamine transporter (Malynn et al., 2013), and promotion of tryptophan depletion (Farzi et al., 2015). AKT1 was more strongly associated with CUMS-induced depression, with a relatively weak correlation with HPRL. Both IL6 and TNF are common inflammatory factors on which PRL has a dual role. There is no doubt that inflammatory factors and depression are closely linked.

The metabolomics results showed that 43 of the three common differential metabolites were up-regulated and one was down-regulated in the three groups of the SNS intervention compared with the model group. These differential metabolites mainly involved the following groups of compounds: amino acids and their metabolites, terpenoids, alkaloids, benzene and its derivatives, heterocyclic compounds, glycerophospholipids, aldehydes, ketones, esters, steroids, alcohols, amines,

organic acids and their derivatives, and glycerolipids. The major metabolic pathways involved in differential metabolites include mainly glycerophospholipid metabolism, glycerolipid metabolism, vitamin digestion and absorption, and fat digestion and absorption.

Glycerophospholipids are the major structural lipid components of eukaryotic cell membranes (H. Wang et al., 2021) and have a wide range of roles in signaling, cell recognition, and membrane function (Ma et al., 2022). It has been suggested that high doses of estrogen may cause depressive-like behavior by interfering with glycerophospholipid metabolism and reversing endogenous cannabinoid signaling pathways (M. Li et al., 2023). By analyzing the gut proteome in a nonhuman primate model of depression, researchers found that differentially expressed proteins related to mitochondrial function and energy metabolism were associated with glycerophospholipid metabolism in the gut of depressed gorillas (X. Chen et al., 2023). Furthermore, glycerophospholipid metabolism plays an important role in the Gut-Liver-Brain axis in depressed mice (Xie et al., 2023). In a study by Liao et al. it was found that administration of a high dose of Banxia Xiexin Tang reduced glycerophospholipid levels in the brain tissue of depressed mice, thereby exerting an antidepressant effect (Liao et al., 2023). Consistent with findings in the literature, the present study found that 1-O-hexadecyl-lyso-sn-glycero-3-phosphocholine and LysoPA (i-24:0/0:0) levels were decreased in the model group as compared to the normal group, but these changes were reversed in the reversed after the intervention of SNS.

Glycerolipids are abundant cellular lipids with important physiological functions in energy metabolism and cell membrane structure (Luo et al., 2023). Studies have found significant changes in the level and structure of 1,2-diacylglycerol in the prefrontal cortex compared to controls in a nonhuman primate model of depression. This altered biochemical structure may affect the fluidity of nerve cell membranes, which in turn affects depressive symptoms (Wu et al., 2022). Notably, MG (18:1/0:0/0:0) belongs to the glycerol ester group and was the only one of the 43 differential metabolites whose levels decreased after treatment with tetrasodium.

The digestion and absorption pathways of vitamins are key processes in the body's acquisition of essential nutrients (Fukui et al., 2022). Vitamin D and vitamin E play key roles in female reproductive function, while vitamin D sufficiency helps to avoid female infertility by protecting cell membranes from oxidative damage and promoting follicular maturation (Alam et al., 2023). Vitamin E increases serum sex hormone levels by enhancing ovarian gonadotropin induction and promoting oocyte maturation (Tao et al., 2023). Most importantly, vitamin B6 can influence hormone secretion, including PRL, by modulating the function of the hypothalamic-pituitary axis (Lu et al., 2022). In addition to this, obesity can cause a decline in gonadotropic function through the influence of sex hormones, manifested as a decrease in serum testosterone and gonadotropin-releasing hormone and luteinizing hormone levels. Obesity can exacerbate insulin resistance in patients with polycystic ovary syndrome, which in turn leads to abnormal androgen secretion (Han et al., 2022). Polycystic ovary syndrome is a common endocrine-metabolic disease and an important cause of female infertility, and obese women are more likely to suffer from this disease (X. Yang et al., 2021).

Of the 44 differential metabolites, 23 were amino acids and their metabolites, but they were not enriched in the relevant pathways. In contrast, only three of the remaining 21 differential metabolites were separately enriched in different pathways, suggesting that they may be key biomarkers for the treatment of hepatic-depressive HPRL by SNS, that is, 1-O-hexadecyl-lysophosphatidylcholine and LysoPA (i-24:0/0:0), and MG (18:1/0:0/0:0). Of the 44 differential metabolites detected, approximately 10 compounds were shown to have anti-inflammatory effects. This finding supports the notion that anti-inflammatory drugs can improve depressive symptoms by reducing inflammatory cytokine levels (Chang et al., 2024), further emphasizing the strong link between depression and chronic inflammation.

The preliminary differential metabolites identified by the criteria of VIP value ≥ 1 and p-value <0.05 appeared to be noteworthy for several substances, namely testosterone, docosahexaenoyl serotonin, and docosahexaenoic acid. The model group of rats showed a significant decrease in testosterone levels after treatment with SNS, consistent with the results of previous studies (Millar et al., 2017). Docosahexaenoic acid plays a key role in neuronal cells and prevents apoptosis by promoting Bcl-2 family protein expression (Díaz et al., 2021). Docosahexaenoyl serotonin, a serotonin derivative, exhibits significant anti-inflammatory effects and may be associated with intestinal diseases such as inflammatory bowel disease (Y. Wang et al., 2017). In the study, curiously, the levels of docosahexaenoids and docosahexaenoyl serotonin were significantly elevated in the model group of rats compared to the blank control group, whereas the levels of these substances were reduced after the treatment, which may be attributed to the activation of self-protective immune mechanisms by the rats in the course of the long-term model preparation, which were weakened by the drug intervention.

Recently, the number of clinical research on HPRL has been on the rise, indicative of a growing patient population. Despite this, there is a notable lack of basic research, and the underlying mechanisms of HPRL remain poorly understood, necessitating a more robust research effort in this field. Presently, treatment options for HPRL are limited, spurring the need for the development of more effective pharmacotherapies that minimize side effects, adverse reactions, and the potential for tolerance. Given the scarcity of foundational research on HPRL, this study is pivotal in advancing our comprehension of its pathogenesis and holds considerable promise for the development of innovative treatment modalities and the improvement of patient well-being.

5. Conclusion

SNS significantly ameliorates hypoprolactinemia linked to liver depression, achieving this at the animal and cellular levels that SNS significantly improved the depression indexes including OFT, TST, SPT, normalized PRL, FSH, E_2 levels and restored ovarian tissue morphology in depression-like rats. In addition, SNS effectively inhibited prolactin secretion from MMQ cells in rats. It may accomplish this by influencing lipid metabolism. Furthermore, the research has identified AKT1, TNF, and IL6 as pivotal therapeutic targets. These findings not only enhance the understanding of the mechanism of action of SNS, but also point out the direction for future research, which is expected to achieve new breakthroughs in improving the treatment of HPRL with liver-depression.

Ethical statements

This study was approved by the Institutional Animal Care and Use Committee of Jiangsu University (Approval number: UJS-IACUC-2023022401).

Author contribution

WX: Formal analysis, Funding acquisition, Methodology, Writing – original draft, Writing – review & editing. ST: Conceptualization, Investigation, Project administration, Writing – original draft. GM: Data curation, Methodology, Writing – original draft. YL: Formal analysis, Investigation, Validation. HQ: Supervision, Visualization, Writing – review & editing. WT: Validation, Visualization.

Declaration of competing interest

The authors declare that they have no known competing financial interests or personal relationships that could have appeared to influence the work reported in this paper.

References

Alam, F., Shahid, M., Riffat, S., Zulkipli, I.N., Syed, F., Ashraf, M., Rehman, R., 2023. SIRT1 and antioxidants in infertile females: exploration of the role of vitamin D. PLoS One 18 (7), e0287727. https://doi.org/10.1371/journal.pone.0287727.

Araujo, A.S.L., Simões, M.J., Araujo-Jr, O.P., Simões, R.S., Baracat, E.C., Nader, H.B., Gomes, R.C.T., 2023. Hyperprolactinemia modifies extracellular matrix components associated with collagen fibrillogenesis in harderian glands of non- and pregnant female mice. Exp. Eye Res. 235, 109612 https://doi.org/10.1016/j.exer.2023.109612.

Bai, Y., Zhang, Y., Li, S., Zhang, W., Wang, X., He, B., Ju, W., 2021. Integrated network pharmacology analysis and experimental validation to investigate the mechanism of zhi-zi-Hou-Po decoction in depression. Front. Pharmacol. 12, 711303 https://doi.org/10.3389/fphar.2021.711303.

Baranoglu Kilinc, Y., Torun, I.E., Kilinc, E., 2024. D2 dopamine receptor-mediated mechanisms of dopaminergic system modulation in in vivo and in vitro experimental models of migraine. Eur. J. Neurosci. 59 (6), 1177–1193. https://doi.org/10.1111/ejn.16106.

Ben-Azu, B., Adebayo, O.G., Moke, E.G., Omogbiya, A.I., Oritsemuelebi, B., Chidebe, E. O., Chukwuma, C., 2023. Geraniol attenuates behavioral and neurochemical impairments by inhibitions of HPA-axis and oxido-inflammatory perturbations in mice exposed to post-traumatic stress disorder. J. Psychiatr. Res. 168, 165–175. https://doi.org/10.1016/j.jpsychires.2023.10.057.

Bernard, V., Young, J., Chanson, P., Binart, N., 2015. New insights in prolactin: pathological implications. Nat. Rev. Endocrinol. 11 (5), 265–275. https://doi.org/10.1038/nrendo.2015.36.

Chang, J., Jiang, T., Shan, X., Zhang, M., Li, Y., Qi, X., Zhao, L., 2024. Pro-inflammatory cytokines in stress-induced depression: novel insights into mechanisms and promising therapeutic strategies. Prog. Neuro-Psychopharmacol. Biol. Psychiatry 131, 110931. https://doi.org/10.1016/j.pnpbp.2023.110931.

Chen, L., Chu, C., Lu, J., Kong, X., Huang, T., Cai, Y.D., 2015. Gene ontology and KEGG pathway enrichment analysis of a drug target-based classification system. PLoS One 10 (5), e0126492. https://doi.org/10.1371/journal.pone.0126492.

Chen, L., Xie, L., Tan, J., Li, N., Luo, Y., Li, M., Wang, Z., 2024. The gut microbiota regulates the depressive-type behaviors and inflammatory processes after severe burn injuries in mice. Heliyon 10 (4), e25617. https://doi.org/10.1016/j.heliyon.2024.e25617.

Chen, X., Liu, Y., Pu, J., Gui, S., Wang, D., Zhong, X., Xie, P., 2023. Proteomics reveals mitochondrial dysfunction and energy metabolism disturbance of intestine in a nonhuman primate model of depression. J. Affect. Disord. 333, 562–570. https://doi.org/10.1016/j.jad.2023.04.031.

De Sousa, S.M.C., Baranoff, J., Rushworth, R.L., Butler, J., Sorbello, J., Vorster, J., Torpy, D.J., 2020. Impulse control disorders in dopamine Agonist-treated hyperprolactinemia: prevalence and risk factors. J. Clin. Endocrinol. Metab. 105 (3) https://doi.org/10.1210/clinem/dgz076.

Deng, D., Cui, Y., Gan, S., Xie, Z., Cui, S., Cao, K., Zhang, R., 2022. Sinisan alleviates depression-like behaviors by regulating mitochondrial function and synaptic plasticity in maternal separation rats. Phytomedicine 106, 154395. https://doi.org/10.1016/j.phymed.2022.154395.

Díaz, M., Mesa-Herrera, F., Marín, R., 2021. DHA and its elaborated modulation of antioxidant defenses of the brain: implications in aging and AD neurodegeneration. Antioxidants 10 (6). https://doi.org/10.3390/antiox10060907.

Dimmer, E.C., Huntley, R.P., Alam-Faruque, Y., Sawford, T., O'Donovan, C., Martin, M. J., Apweiler, R., 2012. The UniProt-GO annotation database in 2011. Nucleic Acids Res. 40 (Database issue), D565–D570. https://doi.org/10.1093/nar/gkr1048.

Farzi, A., Reichmann, F., Meinitzer, A., Mayerhofer, R., Jain, P., Hassan, A.M., Holzer, P., 2015. Synergistic effects of NOD1 or NOD2 and TLR4 activation on mouse sickness behavior in relation to immune and brain activity markers. Brain Behav. Immun. 44, 106–120. https://doi.org/10.1016/j.bbi.2014.08.011.

Feng, H., Zhou, H., Lu, J., Zhang, Q., Tang, X., Shang, Y., 2021. Bu-Shen-Zhu-Yun decoction induces PRLR deubiquitination and JAK2/STAT5 activation via CSN5 in vitro. Aging (Albany NY) 13 (16), 20418–20437. https://doi.org/10.18632/aging.203426.

Fukui, K., Suzuki, Y., Kato, Y., Takeuchi, N., Takenaka, H., Kohno, M., 2022. Effect of extract-added water derived from deep-sea water with different hardness on

cognitive function, motor ability and serum indexes of obese mice. Nutrients 14 (9). https://doi.org/10.3390/nu14091794.

García-Rodrigo, J.F., Ortiz, G., Martínez-Díaz, O.F., Furuzawa-Carballeda, J., Ruíz-Herrera, X., Macias, F., Clapp, C., 2023. Prolactin inhibits or stimulates the inflammatory response of joint tissues in a cytokine-dependent manner. Endocrinology 164 (12). https://doi.org/10.1210/endocr/bqad156.

Gragnoli, C., Reeves, G.M., Reazer, J., Postolache, T.T., 2016. Dopamine-prolactin pathway potentially contributes to the schizophrenia and type 2 diabetes comorbidity. Transl. Psychiatry 6 (4), e785. https://doi.org/10.1038/tp.2016.50.

Han, Y., Lin, B., Lu, W., Wang, X., Tang, W., Tao, X., Liu, C., 2022. Time-restricted feeding improves metabolic and endocrine profiles in mice with polycystic ovary syndrome. Front. Endocrinol. 13, 1057376 https://doi.org/10.3389/fendo.2022.1057376.

Hummel, W.P., Clark, M.R., Talbert, L.M., 1990. Transient hyperprolactinemia during cycle stimulation and its influence on oocyte retrieval and fertilization rates. Fertil. Steril. 53 (4), 677–681. https://doi.org/10.1016/s0015-0282(16)53463-3.

Kim, S.I., Yoon, J.H., Park, D.C., Yang, S.H., Kim, Y.I., 2023. What is the optimal prolactin cutoff for predicting the presence of a pituitary adenoma in patients with polycystic ovary syndrome? Int. J. Med. Sci. 20 (4), 463–467. https://doi.org/10.7150/ijms.80891.

Li, M., Zhang, J., Chen, W., Liu, S., Liu, X., Ning, Y., Zhao, Y., 2023. Supraphysiologic doses of 17β-estradiol aggravate depression-like behaviors in ovariectomized mice possibly via regulating microglial responses and brain glycerophospholipid metabolism. J. Neuroinflammation 20 (1), 204. https://doi.org/10.1186/s12974-023-02889-5.

Li, Z., Zhao, Y., Cheng, J., Xu, L., Wen, X., Sun, Y., He, Y., 2022. Integrated plasma metabolomics and gut microbiota analysis: the intervention effect of jiawei Xiaoyao san on liver depression and spleen deficiency liver cancer rats. Front. Pharmacol. 13, 906256 https://doi.org/10.3389/fphar.2022.906256.

Liao, X.X., Hu, K., Xie, X.H., Wen, Y.L., Wang, R., Hu, Z.W., Zhou, J.J., 2023. Banxia Xiexin decoction alleviates AS co-depression disease by regulating the gut microbiome-lipid metabolic axis. J. Ethnopharmacol. 313, 116468 https://doi.org/10.1016/j.jep.2023.116468.

Lim, C.M., Carey, M., Williams, P.N., Koidis, A., 2021. Rapid classification of commercial teas according to their origin and type using elemental content with X-ray fluorescence (XRF) spectroscopy. Curr. Res. Food Sci. 4, 45–52. https://doi.org/10.1016/j.crfs.2021.02.002.

Liu, J., Fang, Y., Cui, L., Wang, Z., Luo, Y., Gao, C., Zhou, T., 2022. Butyrate emerges as a crucial effector of Zhi-Zi-Chi decoctions to ameliorate depression via multiple pathways of brain-gut axis. Biomed. Pharmacother. 149, 112861 https://doi.org/10.1016/j.biopha.2022.112861.

Liu, L., Yang, F., Jing, Y., Xin, L., 2019. Data mining in Xu Runsan's Traditional Chinese Medicine practice: treatment of chronic pelvic pain caused by pelvic inflammatory disease. J. Tradit. Chin. Med. 39 (3), 440–450.

Liu, M., Yang, T., Zhao, X., Wang, Y., Li, M., Wang, Y., Zhou, J., 2024. Classification and characterization on sorghums based on HS-GC-IMS combined with OPLS-DA and GA-PLS. Curr. Res. Food Sci. 8, 100692 https://doi.org/10.1016/j.crfs.2024.100692.

Liu, X., Wu, X., Wang, S., Qin, X., 2023. Gut microbiome and tissue metabolomics reveal the compatibility effects of Xiaoyaosan on depression based on "gut-liver-kidney" axis. Phytomedicine 111, 154628. https://doi.org/10.1016/j.phymed.2022.154628.

Liu, Y., Lv, B., Tang, K., Qu, H., Yu, F., Shi, Y., 2023. Si-Ni-San reverses dietary fat absorption defects in a murine model of depression. Biomed. Pharmacother. 168, 115677 https://doi.org/10.1016/j.biopha.2023.115677.

Lu, Z., Sun, Y., Zhang, Y., Chen, Y., Guo, L., Liao, Y., Yue, W., 2022. Pharmacological treatment strategies for antipsychotic-induced hyperprolactinemia: a systematic review and network meta-analysis. Transl. Psychiatry 12 (1), 267. https://doi.org/10.1038/s41398-022-02027-4.

Luo, Y., Zhong, Z., Li, H., Wang, L., Guo, D., Dong, X., Meng, P., 2023. Integrating serum metabolomics and network analysis to explore the antidepressant activity of crocin in rats with chronic unexpected mild stress-induced depression. Pharm. Biol. 61 (1), 1414–1430. https://doi.org/10.1080/13880209.2023.2246531.

Ma, F., Sun, M., Song, Y., Wang, A., Jiang, S., Qian, F., Tuo, Y., 2022. Lactiplantibacillus plantarum-12 alleviates inflammation and colon cancer symptoms in AOM/DSS-Treated mice through modulating the intestinal microbiome and metabolome. Nutrients 14 (9). https://doi.org/10.3390/nu14091916.

Malynn, S., Campos-Torres, A., Moynagh, P., Haase, J., 2013. The pro-inflammatory cytokine TNF-α regulates the activity and expression of the serotonin transporter (SERT) in astrocytes. Neurochem. Res. 38 (4), 694–704. https://doi.org/10.1007/s11064-012-0967-y.

Mastnak, L., Herman, R., Ferjan, S., Janež, A., Jensterle, M., 2023. Prolactin in polycystic ovary syndrome: metabolic effects and therapeutic prospects. Life 13 (11). https://doi.org/10.3390/life13112124.

Millar, R.P., Sonigo, C., Anderson, R.A., George, J., Maione, L., Brailly-Tabard, S., Young, J., 2017. Hypothalamic-pituitary-ovarian Axis reactivation by kisspeptin-10 in hyperprolactinemic women with chronic amenorrhea. J Endocr Soc 1 (11), 1362–1371. https://doi.org/10.1210/js.2017-00328.

Moreno-Carranza, B., Goya-Arce, M., Vega, C., Adán, N., Triebel, J., López-Barrera, F., Clapp, C., 2013. Prolactin promotes normal liver growth, survival, and regeneration in rodents: effects on hepatic IL-6, suppressor of cytokine signaling-3, and angiogenesis. Am. J. Physiol. Regul. Integr. Comp. Physiol. 305 (7), R720–R726. https://doi.org/10.1152/ajpregu.00282.2013.

Ogata, H., Goto, S., Sato, K., Fujibuchi, W., Bono, H., Kanehisa, M., 1999. KEGG: Kyoto Encyclopedia of genes and Genomes. Nucleic Acids Res. 27 (1), 29–34. https://doi.org/10.1093/nar/27.1.29.

Ru, J., Li, P., Wang, J., Zhou, W., Li, B., Huang, C., Yang, L., 2014. TCMSP: a database of systems pharmacology for drug discovery from herbal medicines. J. Cheminf. 6, 13. https://doi.org/10.1186/1758-2946-6-13.

Shannon, P., Markiel, A., Ozier, O., Baliga, N.S., Wang, J.T., Ramage, D., Ideker, T., 2003. Cytoscape: a software environment for integrated models of biomolecular interaction networks. Genome Res. 13 (11), 2498–2504. https://doi.org/10.1101/gr.1239303.

Shen, C., Cao, K., Cui, S., Cui, Y., Mo, H., Wen, W., Shi, Y., 2020. SiNiSan ameliorates depression-like behavior in rats by enhancing synaptic plasticity via the CaSR-PKC-ERK signaling pathway. Biomed. Pharmacother. 124, 109787 https://doi.org/10.1016/j.biopha.2019.109787.

Stelzer, G., Rosen, N., Plaschkes, I., Zimmerman, S., Twik, M., Fishilevich, S., Lancet, D., 2016. The GeneCards suite: from gene data mining to disease genome sequence analyses. Curr Protoc Bioinformatics 54. https://doi.org/10.1002/cpbi.5, 1.30.31-1.30.33.

Su, L., Mao, J., Hao, M., Lu, T., Mao, C., Ji, D., Fei, C., 2019. Integrated plasma and bile metabolomics based on an UHPLC-Q/TOF-MS and network pharmacology approach to explore the potential mechanism of schisandra chinensis-protection from acute alcoholic liver injury. Front. Pharmacol. 10, 1543. https://doi.org/10.3389/fphar.2019.01543.

Szklarczyk, D., Gable, A.L., Lyon, D., Junge, A., Wyder, S., Huerta-Cepas, J., Mering, C. V., 2019. STRING v11: protein-protein association networks with increased coverage, supporting functional discovery in genome-wide experimental datasets. Nucleic Acids Res. 47 (D1), D607–d613. https://doi.org/10.1093/nar/gky1131.

Szukiewicz, D., 2024. Current insights in prolactin signaling and ovulatory function. Int. J. Mol. Sci. 25 (4) https://doi.org/10.3390/ijms25041976.

Tang, C., Sun, R., Wen, G., Zhong, C., Yang, J., Zhu, J., Ma, C., 2019. Bromocriptine and cabergoline induce cell death in prolactinoma cells via the ERK/EGR1 and AKT/mTOR pathway respectively. Cell Death Dis. 10 (5), 335. https://doi.org/10.1038/s41419-019-1526-0.

Tao, Y., Pan, Y., Wang, Q., Lu, S., Li, Y., Liu, W., Xu, P., 2023. Vitamin E ameliorates impaired ovarian development, oxidative stress, and disrupted lipid metabolism in Oreochromis niloticus fed with a diet containing olive oil instead of fish oil. Antioxidants 12 (8). https://doi.org/10.3390/antiox12081524.

Tian, X., Wang, G., Teng, F., Xue, X., Pan, J., Mao, Q., Ma, K., 2023. Zhi Zi Chi decoction (Gardeniae fructus and semen Sojae Praeparatum) attenuates anxious depression via modulating microbiota-gut-brain axis in corticosterone combined with chronic restraint stress-induced mice. CNS Neurosci. Ther. https://doi.org/10.1111/cns.14519.

Vander Borght, M., Wyns, C., 2018. Fertility and infertility: definition and epidemiology. Clin. Biochem. 62, 2–10. https://doi.org/10.1016/j.clinbiochem.2018.03.012.

Wang, H., Liu, J., He, J., Huang, D., Xi, Y., Xiao, T., Chen, X., 2022. Potential mechanisms underlying the therapeutic roles of sinisan formula in depression: based on network pharmacology and molecular docking study. Front. Psychiatr. 13, 1063489 https://doi.org/10.3389/fpsyt.2022.1063489.

Wang, H., Wang, Z., Liu, Z., Wang, K., Xu, W., 2021. Membrane disruption of Fusarium oxysporum f. sp. niveum induced by myriocin from Bacillus amyloliquefaciens LZN01. Microb. Biotechnol. 14 (2), 517–534. https://doi.org/10.1111/1751-7915.13659.

Wang, W., Ige, O.O., Ding, Y., He, M., Long, P., Wang, S., Wen, X., 2023. Insights into the potential benefits of triphala polyphenols toward the promotion of resilience against stress-induced depression and cognitive impairment. Curr. Res. Food Sci. 6, 100527 https://doi.org/10.1016/j.crfs.2023.100527.

Wang, Y., Balvers, M.G.J., Hendriks, H.F.J., Wilpshaar, T., van Heek, T., Witkamp, R.F., Meijerink, J., 2017. Docosahexaenoyl serotonin emerges as most potent inhibitor of IL-17 and CCL-20 released by blood mononuclear cells from a series of N-acyl serotonins identified in human intestinal tissue. Biochim. Biophys. Acta Mol. Cell Biol. Lipids 1862 (9), 823–831. https://doi.org/10.1016/j.bbalip.2017.05.008.

Wei, Y., La, L., Wang, L., Batey, R., Wang, C., Li, Y., 2017. Paeoniflorin and liquiritin, two major constituents in Chinese herbal formulas used to treat hyperprolactinemia-associated disorders, inhibits prolactin secretion in prolactinoma cells by different mechanisms. J. Ethnopharmacol. 204, 36–44. https://doi.org/10.1016/j.jep.2017.03.054.

Wu, J., Chai, T., Zhang, H., Huang, Y., Perry, S.W., Li, Y., Xie, P., 2022. Changes in gut viral and bacterial species correlate with altered 1,2-diacylglyceride levels and structure in the prefrontal cortex in a depression-like non-human primate model. Transl. Psychiatry 12 (1), 74. https://doi.org/10.1038/s41398-022-01836-x.

Xiao, G., Xu, A., Jiang, J., Chen, Z., Li, Y., Li, S., Bi, X., 2023. Metabolomics analysis delineates the therapeutic effects of Yinlan Tiaozhi capsule on triton WR-1339-induced hyperlipidemia in mice. Front. Pharmacol. 14, 1252146 https://doi.org/10.3389/fphar.2023.1252146.

Xie, J., Zhong, Q., Wu, W.T., Chen, J.J., 2023. Multi-omics data reveals the important role of glycerophospholipid metabolism in the crosstalk between gut and brain in depression. J. Transl. Med. 21 (1), 93. https://doi.org/10.1186/s12967-023-03942-w.

Xu, W., Du, X., Li, J., Zhang, Z., Ma, X., Luo, D., Sun, Q., 2022a. SiNiSan alleviates liver injury by promoting hepatic stem cell differentiation via Wnt/β-catenin signaling pathway. Phytomedicine 99, 153969. https://doi.org/10.1016/j.phymed.2022.153969.

Xu, W., Zhang, Z., Lu, Y., Li, M., Li, J., Tao, W., 2022b. Traditional Chinese medicine Tongxie Yaofang treating irritable bowel syndrome with diarrhea and type 2 diabetes mellitus in rats with liver-depression and spleen-deficiency: a preliminary study. Front. Nutr. 9, 968930 https://doi.org/10.3389/fnut.2022.968930.

Yang, X., Wu, R., Qi, D., Fu, L., Song, T., Wang, Y., Shi, Y., 2021. Profile of bile acid metabolomics in the follicular fluid of PCOS patients. Metabolites 11 (12). https://doi.org/10.3390/metabo11120845.

Yang, Y., Zhou, D., Min, S., Liu, D., Zou, M., Yu, C., Hong, R., 2024. Ciprofol ameliorates ECS-induced learning and memory impairment by modulating aerobic glycolysis in the hippocampus of depressive-like rats. Pharmacol. Biochem. Behav. 239, 173775 https://doi.org/10.1016/j.pbb.2024.173775.

Ye, L., Wu, J., Liu, Z., Deng, D., Bai, S., Yang, L., Zhao, J., 2023. Si-Ni-San alleviates early life stress-induced depression-like behaviors in adolescence via modulating Rac1 activity and associated spine plasticity in the nucleus accumbens. Front. Pharmacol. 14, 1274121 https://doi.org/10.3389/fphar.2023.1274121.

Ye, Q., Zhang, Q.Y., Zheng, C.J., Wang, Y., Qin, L.P., 2010. Casticin, a flavonoid isolated from Vitex rotundifolia, inhibits prolactin release in vivo and in vitro. Acta Pharmacol. Sin. 31 (12), 1564–1568. https://doi.org/10.1038/aps.2010.178.

Zeng, Y., Huang, Q., Zou, Y., Tan, J., Zhou, W., Li, M., 2023. The efficacy and safety of quinagolide in hyperprolactinemia treatment: a systematic review and meta-analysis. Front. Endocrinol. 14, 1027905 https://doi.org/10.3389/fendo.2023.1027905.

Zhai, S.Y., Gu, H.W., Wang, C., Li, Y.S., Tang, H.B., 2024. Gynura procumbens and selected metabolites: amelioration of depressive-like behaviors in mice and risperidone-induced hyperprolactinemia in rats. Biomed. Pharmacother. 173, 116361 https://doi.org/10.1016/j.biopha.2024.116361.

Zhang, H., Wang, C., Li, X., Zhang, Y., 2016. Effects of pterostilbene on treating hyperprolactinemia and related mechanisms. Am J Transl Res 8 (7), 3049–3055.

Zhang, M., Wu, W., Huang, C., Cai, T., Zhao, N., Liu, S., Yang, S., 2022. Shuxie-1 decoction alleviated CUMS -induced liver injury via IL-6/JAK2/STAT3 signaling. Front. Pharmacol. 13, 848355 https://doi.org/10.3389/fphar.2022.848355.

Zhang, M.J., Song, M.L., Zhang, Y., Yang, X.M., Lin, H.S., Chen, W.C., He, S.Q., 2023. SNS alleviates depression-like behaviors in CUMS mice by regulating dendritic spines via NCOA4-mediated ferritinophagy. J. Ethnopharmacol. 312, 116360 https://doi.org/10.1016/j.jep.2023.116360.

Zhang, S., Liu, B., Huang, L., Zhang, R., An, L., Liu, Z., 2023. Metabolomics reveals that chronic restraint stress alleviates carbon tetrachloride-induced hepatic fibrosis through the INSR/PI3K/AKT/AMPK pathway. J. Mol. Med. (Berl.). https://doi.org/10.1007/s00109-023-02395-4.

Zhao, W., Ji, C., Zheng, J., Zhou, S., Tian, J., Han, Y., Qin, X., 2024. Effects of Xiaoyao San on exercise capacity and liver mitochondrial metabolomics in rat depression model. Chin Herb Med 16 (1), 132–142. https://doi.org/10.1016/j.chmed.2023.09.004.

Zheng, Y., Zhang, J., Huang, W., Zhong, L.L.D., Wang, N., Wang, S., Wang, Z., 2021. Sini san inhibits chronic psychological stress-induced breast cancer stemness by suppressing cortisol-mediated GRP78 activation. Front. Pharmacol. 12, 714163 https://doi.org/10.3389/fphar.2021.714163.

Zhu, H., Zhang, Y., Duan, Y., Pei, K., Tu, S., Chen, Y., Cai, H., 2023. Pharmacokinetic evaluation of Sinisan containing vinegar-processed products in depressive rats, a comprehensive perspective of 'individual herb, herb-pair, and herbal formula'. J. Ethnopharmacol. 317, 116817 https://doi.org/10.1016/j.jep.2023.116817.

Zorzi, E., Bonvini, P., 2011. Inducible hsp70 in the regulation of cancer cell survival: analysis of chaperone induction, expression and activity. Cancers 3 (4), 3921–3956. https://doi.org/10.3390/cancers3043921.